EPM–RT–2009-06

PREDICTION OF THE RESPONSE OF A THIN STRUCTURE SUBJECTED TO A TURBULENT BOUNDARY-LAYER-INDUCED RANDOM PRESSURE FIELD

Mitra Esmailzadeh, Aouni A. Lakis
Département de Génie mécanique
École Polytechnique de Montréal

Août 2009

Poly

ÉCOLE POLYTECHNIQUE MONTRÉAL

EPM-RT-2009-06

Prediction of the response of a thin structure subjected to a turbulent boundary-layer-induced random pressure field

Mitra Esmailzadeh, Ph.D., assistante de recherche

Prof. Aouni A. Lakis, Ph.D.

Département de génie mécanique,
École Polytechnique de Montréal
C.P. 6079, Succursale Centre Ville, Montréal, Québec H3C 3A7

Août 2009

Dépôt légal :
Bibliothèque nationale du Québec, 2009
Bibliothèque nationale du Canada, 2009

EPM-RT-2009-06

Prediction of the response of a thin structure subjected to a turbulent boundary-layer-induced random pressure field

Par : Mitra Esmailzadeh, Aouni A. Lakis
Département de génie mécanique
École Polytechnique de Montréal

Abstract

A method capable of predicting the root mean square displacement response of a thin structure subjected to a turbulent boundary-layer-induced random pressure field is presented. The basic formulation of the dynamic problem is an efficient approach combining classic thin shell theory and the finite element method, in which the finite elements are flat rectangular elements with six degrees of freedom per node. The displacement functions are derived from thin shell theory. Description of the turbulent pressure field is based on the Corcos formulation for cross spectral density of pressure fluctuations. A numerical approach is proposed to obtain the total root mean square displacements of the structure. Exact integration over surface and frequency leads to an expression for the response in terms of the characteristics of the structure and flow. An in-house program based on the presented method was developed. The total root mean square displacements of a thin plate under different boundary conditions subjected to a turbulent boundary layer were calculated and illustrated as a function of free stream velocity and damping ratio and the effects of flow direction on the response were also investigated. In addition, the power spectral densities of the displacements of an SFSF plate subjected to a fully developed turbulent flow were studied. The total root mean square radial displacement of a thin cylindrical shell was obtained and compared favorably with that in the literature.

1. Introduction

Responses of structures subjected to turbulent boundary layer excitation have long been of great practical importance in engineering. Some examples are; marine applications, aircraft structures and power plants. Random pressure induced by a fully developed turbulent boundary layer is a frequent source of excitation and can cause low-amplitude vibration and eventually long-term structural fatigue. For this reason, determination of the response of structures subjected to boundary layer pressure fields is of importance.

Experimental and theoretical investigations of induced random pressure fields have been carried out by many researchers including Corcos [1,2], Maestrello [3], Farabee and Casarella [4], etc. Investigations of the fluctuating wall pressure beneath a turbulent boundary layer have also been conducted by many researchers for fully developed turbulent pipe flow [5,6] and for turbulent boundary layers on flat plates [7,8]. Blake [9] includes a chapter on structural response to turbulent wall flow in his book. He determined relationships for the mean-square modal velocity and displacement of one single mode of a panel in terms of the auto-spectral density of modal pressure.

Experimental works have mainly concentrated on the power spectral density of the pressure and space-time cross correlation functions. Most of the studies in the literature are devoted to investigating pressure fluctuations beneath a turbulent boundary layer, and studies on the displacement response of an elastic structure to these excitations are scarce. A simply supported uniform thin cylindrical shell subjected to a turbulent boundary layer was modeled theoretically by Cottis and Jasonides [10]. They derived a general expression for the space-time correlation of the response for both arbitrary and boundary-layer-induced

pressure fields but they did not proceed to evaluate the mean square value of response, nor did they undertake numerical solution of the problem. Their work was later extended to orthotropic shells [11]. To our knowledge, the first attempt to make a comparison of measured and predicted pipe vibration was made by Clinch [12]. He considered simply supported thin cylindrical shells which he analyzed using Powell's joint-acceptance method. In the analysis he assumed that the areas over which the wall pressure fluctuations are correlated are small compared with pipe dimensions. More importantly, he considered the response only in the high modes of the shell, where resonances are so close to one another that a continuous curve of response versus frequency may be assumed. He then compared his theoretical results to his own experimental data for a long, slender, thin cylinder conveying water. The average root mean square wall displacement displayed good agreement between theory and experiment at high frequencies. The limitation of his theory is that it applies only for high frequencies. However, it is worth mentioning that only the first resonance frequencies of the shell make a significant contribution to the response due to turbulent flow. Following Clinch's study, Lakis and Païdoussis presented [13] a theory to predict the displacement response of a uniform or axially non-uniform thin cylindrical shell to an arbitrary random pressure field, and to a pressure field arising from the turbulent boundary layer of an internal subsonic flow. They obtained the root mean square (rms) displacements of the shell for a pressure field originating from the turbulent boundary layer of a subsonic internal flow at a specific circumferential wavenumber as well as the total displacement response by summation over all circumferential modes. Curling and Païdoussis [14] investigated an analytical solution to obtain the power spectral density (PSD) of the displacements of bundles of cylinders in turbulent axial flow. They calculated

PSD of mid-cylinder displacements and compared results with experimental measurements obtained by Gagnon and Païdoussis.

Innovative and fast solutions for the stochastic response of a plate have been carried out by many researchers [15-19]. Birgersson et al. [15] used spectral finite element and dynamic stiffness methods to analyze the autospectral density of the velocity of a plate due to a turbulent boundary layer. They utilized an approach in which the cross spectral density of the response was determined by a single integration over all wavenumbers rather than double integrals over the surface. Finnveden et al. [16] investigated the vibration response of a plate excited by a turbulent boundary layer experimentally and numerically. The vibration response of the velocity of a thin-walled plate was measured and then predicted using wall pressure models. The measured response agreed with existing models in a low frequency regime. Mazzoni [17] proposed a deterministic model based on an analytical wavenumber integration procedure to predict the response of a thin elastic plate subjected to both a turbulent flow of fluid at a low Mach number and acoustic noise. The power spectrum of the acceleration of the fluid-loaded plate subjected to a turbulent boundary layer was obtained and compared with that obtained with using a classical random approach. Vitiello et al. [18] developed a procedure to evaluate the aeroelastic response of a flat plate excited by a turbulent boundary layer. De Rosa and Franco [19] presented an exact and predictive response for a simply supported plate wetted on one side subjected to a turbulent boundary layer. Autospectral velocity of thin plates excited by low-speed turbulent boundary layer flow was analyzed numerically and experimentally by Hambric et al. [20].

A cylindrical finite element was developed by one of the authors of this article, in which

displacement functions were derived from shell equations of motion instead of using polynomial displacement functions [21,22]. Prior to the work presented herein, this element could only be applied to cylindrical, conical or spherical shells since it is a cylindrical frustum. Based on this element, another work has been developed by one of the authors of this paper to predict the response of a thin cylindrical shell subjected to random pressure fluctuations arising from a turbulent boundary layer [13].

In this paper we develop a general method to model any kind of thin elastic structure subjected to an arbitrary random pressure field and subsequently to a pressure field arising from a fully developed turbulent boundary layer. The finite element used in this study is based on a previously developed method to study dynamic behavior of a thin structure subjected to stationary fluid [23,24]. In this approach a flat rectangular element with six degrees of freedom per node was developed using a combination of Sanders' thin shell theory and the finite element method. Since the transverse displacement function is derived from thin plate theory this method may be easily adapted to take hydrodynamic effects into account. Moreover, this method is capable of calculating both high and low frequencies with high accuracy. This capability is normally of little interest in free vibration analysis, but it is of considerable importance for determining the response of structures subjected to random pressure fields such as those generated by turbulent flow. A continuous random pressure field is transformed into a discrete force field acting at each node of the finite element. Structural response to turbulence-induced excitation forces is calculated using random vibration theory. Corcos formulation for cross spectral density of the pressure fluctuations was adopted to describe the turbulent pressure field. A numerical approach is proposed to obtain the magnitude of the random response. Exact integration over surface

and frequency was carried out analytically and an expression for the root mean square displacement response was obtained in terms of the characteristics of the structure and flow.

An in-house program was developed to predict the root mean square displacement response of a thin structure to a random pressure field arising from a turbulent boundary layer. In order to demonstrate the applicability of the proposed method, a thin plate under different boundary conditions was investigated. Accuracy of the proposed method was also verified for a cylindrical shell case. A thin cylindrical shell was analyzed and compared with the results obtained by Lakis and Païdoussis [13]. In our proposed method, the Corcos lateral and longitudinal correlations were used, but in Lakis' results Bakewell correlations were employed. Even though different correlations were adapted in the numerical calculation, good agreement was found. It should be noted that Lakis validated his results by verifying with Clinch's experimental measurements and good agreement was obtained [13]. In other words, comparison with Clinch's experimental measurements shows that our method is sound. It seems that their work is the only case in the literature that calculates the total rms displacement of a shell subjected to a random pressure field arising from a boundary layer induced by turbulent flow. Comparisons with experimental measurements are scarce in the literature. Thus, this case study is undertaken in order to validate our method. As mentioned earlier, research has been conducted on auto-spectral density of the response of a plate but the vibration amplitude (total rms displacement) was not investigated.

Assumptions introduced into the theory are as follows: (1) the plate is assumed to be thin; (2) the pressure field is assumed to be stationary, ergodic and homogeneous; (3) the

damping matrix is assumed to be proportional to mass and stiffness matrices in order to uncouple the equations of motion; (4) the turbulent boundary layer is fully developed; (5) acoustic pressure fluctuations induced by flow at moderate speeds are very small compared to turbulent pressure fluctuations, therefore we assume excitation only arises from pressure fluctuations in the turbulent boundary layer; (6) the compressibility effect is negligible; (7) flow is subsonic and Mach number is below 0.3; (8) pressure drop over the length of the plate is sufficiently small for the mean pressure to be considered constant over this length; (9) influence of the structural vibration induced by the fluctuating pressure field on the boundary layer is neglected due to its sufficiently small amplitude; and (10) non-inertial dynamic effects of the flow are negligible.

2. Equation of motion

Dynamic behavior of a structure subjected to arbitrary loads is governed by the following equation:

$$[\mathbf{M}]\{\ddot{\boldsymbol{\delta}}\} + [\mathbf{C}]\{\dot{\boldsymbol{\delta}}\} + [\mathbf{K}]\{\boldsymbol{\delta}\} = \{\mathbf{F}(x, y, t)\}, \tag{1}$$

where **M**, **C** and **K** are the global mass, damping and stiffness matrices of the system, respectively, $\boldsymbol{\delta}$, $\dot{\boldsymbol{\delta}}$ and $\ddot{\boldsymbol{\delta}}$ are the global displacement, velocity and acceleration vectors, respectively and $\mathbf{F}(x, y, t)$ is a vector of external forces as a function of space and time.

Eq. (1) is quite general. In this paper we base our theory on a developed method for analysis of a thin plate in a vacuum and in inviscid incompressible stationary fluid [23,24]. Global mass and stiffness matrices were determined using this method to obtain the free

vibration characteristics of such plates. To briefly summarize; this theory was developed using a combination of classic thin plate theory and finite element analysis in which the finite elements were four-noded flat rectangular elements with six degrees of freedom per node, representing the in-plane and out-of-plane displacements and their spatial derivatives. The displacement functions were derived from Sanders' thin shell equations instead of the usual and more arbitrary interpolating polynomials. To establish the equilibrium equations for rectangular thin plates, Sanders' equations for cylindrical shells are used assuming the radius to be infinite. Both membrane and bending effects are taken into account in this theory to enable the element to model curved structures as well. It is worth mentioning that Sanders based his equations on Love's first approximation theory but he demonstrated that all strains vanish for rigid body motion, which satisfies the convergence criteria of the finite element. The structural mass and stiffness matrices were determined by exact analytical integration. The fluid pressure applied on the structure was determined by combining the velocity potential function, Bernoulli's equation and the impermeability condition and was expressed as a function of acceleration of the normal displacement of the structure and the inertial force of the quiescent fluid. An analytical integration of the fluid pressure over the element produced the virtual added-mass matrix of stationary fluid.

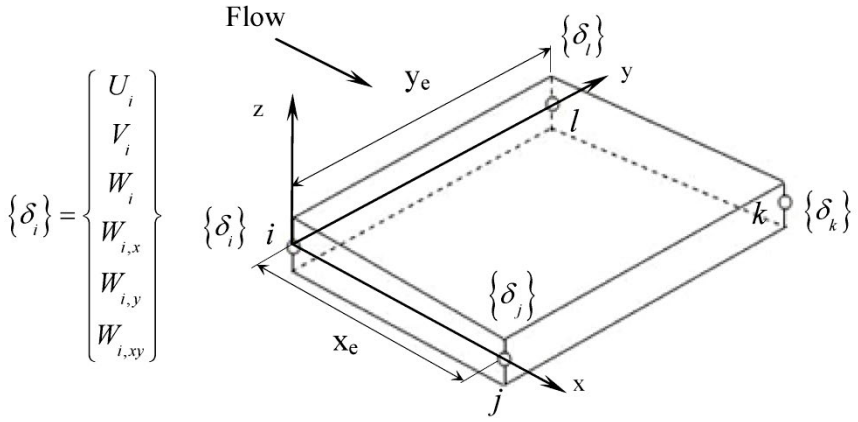

Fig. 1. Flat rectangular element.

The geometry of the structure element used in this analysis is shown in Fig. 1. The nodal displacement vector at node *i*, $\boldsymbol{\delta}_i$ is defined by

$$\{\boldsymbol{\delta}_i\} = \left\{ U_i \quad V_i \quad W_i \quad \partial W_i/\partial x \quad \partial W_i/\partial y \quad \partial^2 W_i/\partial x \partial y \right\}^{\mathrm{T}}, \tag{2}$$

where U_i and V_i are the in-plane displacements of the plate reference surface in the *x*- and *y*- directions, respectively, W_i represents the radial displacement of the plate middle surface, $\partial W_i/\partial x$ and $\partial W_i/\partial y$ are the first derivatives of the radial displacement with respect to *x* and *y*, respectively, and $\partial^2 W_i/\partial x \partial y$ is the cross derivative of the radial displacement with respect to *x* and *y* at node *i*.

The displacement vector $\boldsymbol{\delta}$, for a plate subdivided into finite elements having *n* nodes has the form

$$\{\boldsymbol{\delta}\} = \left\{ \{\boldsymbol{\delta}_1\}^{\mathrm{T}}, \{\boldsymbol{\delta}_2\}^{\mathrm{T}}, ..., \{\boldsymbol{\delta}_n\}^{\mathrm{T}} \right\}^{\mathrm{T}}. \tag{3}$$

3. Uncoupling the equations of motion

All the terms in Eq. (1) have now been defined except for the damping matrix, which will not be given an explicit form for reasons to become obvious below. Before proceeding with a discussion of the response of the plate to random pressure fields we need to uncouple the equation of motion.

The plate response $\boldsymbol{\delta}(x,y,t)$ at any point *x, y* and at any time *t* may be expressed as a normal mode expansion in terms of the generalized coordinates $\mathbf{q}(t)$ and the modal matrix as follows:

$$\{\boldsymbol{\delta}(x,y,t)\} = \left[\{\boldsymbol{\Phi}_1\},\{\boldsymbol{\Phi}_2\},...,\{\boldsymbol{\Phi}_N\}\right]\{\mathbf{q}(t)\} = \left[\boldsymbol{\Phi}(x,y)\right]\{\mathbf{q}(t)\}, \tag{4}$$

where $[\boldsymbol{\Phi}(x,y)]$ is the modal matrix in a vacuum, which consists of the orthogonal eigenvectors $\{\boldsymbol{\Phi}_i\}$, and *N* is the number of mode shapes to be used in the analysis.

Substituting the above relationship into the equation of motion and pre-multiplying by $\boldsymbol{\Phi}^{\mathrm{T}}$, the following equation is obtained:

$$[\bar{\mathbf{M}}]\{\ddot{\mathbf{q}}\} + [\bar{\mathbf{C}}]\{\dot{\mathbf{q}}\} + [\bar{\mathbf{K}}]\{\mathbf{q}\} = \left[\boldsymbol{\Phi}\right]^{\mathrm{T}}\{\mathbf{F}\}, \tag{5}$$

where $\bar{\mathbf{M}} = \boldsymbol{\Phi}^{\mathrm{T}}\mathbf{M}\boldsymbol{\Phi}$ and $\bar{\mathbf{K}} = \boldsymbol{\Phi}^{\mathrm{T}}\mathbf{K}\boldsymbol{\Phi}$ are the generalized mass and stiffness matrices, respectively. Due to orthogonality of the normal modes, $\bar{M}$ and $\bar{K}$ are diagonal matrices and the generalized damping matrix $\bar{\mathbf{C}} = \boldsymbol{\Phi}^{\mathrm{T}}\mathbf{C}\boldsymbol{\Phi}$ will be a diagonal matrix if it is taken to be proportional to $\bar{\mathbf{M}}$ and $\bar{\mathbf{K}}$, or a linear combination of these. The viscous damping type of structural damping is adopted in the equation of motion. Denoting the *r*th diagonal term of $\bar{\mathbf{C}}$ by $\bar{C}_r = 2\zeta_r\sqrt{\bar{K}_r\bar{M}_r}$, $\bar{M}_r$ and $\bar{K}_r$ being the corresponding terms of $\bar{\mathbf{M}}$ and $\bar{\mathbf{K}}$, and ζ_r

being the *r*th generalized damping ratio and introducing these into Eq. (1) leads to the uncoupled set of equations:

$$\ddot{q}_r + 4\pi\zeta_r f_r \dot{q}_r + 4\pi^2 f_r^2 q_r = \frac{1}{\bar{M}_r}\{\mathbf{\Phi}\}_r^{\mathrm{T}}\{\mathbf{F}\}, \qquad r = 1, 2, ..., N, \tag{6}$$

where f_r is the *r*th natural frequency in Hz, $\bar{M}_r$ is the *r*th element of the generalized mass matrix and *N* is the number of mode shapes chosen for evaluation.

Upon solving the above equation the response at a typical node *g*, $\boldsymbol{\delta}_g$ in terms of the generalized coordinates is found:

$$\left\{\boldsymbol{\delta}_g(x,y,t)\right\} = \sum_{r=1}^{N}\left\{\mathbf{\Phi}_{gr}(x,y)\right\}\left\{q_r(t)\right\}, \tag{7}$$

where $\mathbf{\Phi}_{gr}(x,y)$ is the *r*th mode shape at node *g* with $q_r(t)$ being the associated generalized coordinates. This is the instantaneous response due to an arbitrary force vector.

4. Representation of a continuous random pressure field at the nodal points

The continuous random pressure field of the deformable body will be approximated using a finite set of discrete forces and moments acting at the nodal points. The plate is divided into finite elements, each of which is a rectangular flat element. A pressure field is considered to be acting on an area S_c surrounding the node *c* of the coordinates l_c and d_c as shown in Fig. 2. This area S_c is delimited by the positions l_c' and l_c'' with respect to the origin in the *x*-direction and d_c' and d_c'' with respect to the origin in the *y*-direction. It is therefore possible to determine the pressure distribution acting over the area S_c in terms of

a lateral force. The lateral force acting at an arbitrary point, A, on the area S_c is given by (see Fig. 2)

$$F_A(t) = \int_{d'_c}^{d''_c} \int_{l'_c}^{l''_c} P(x,y,t)\mathrm{d}x\,\mathrm{d}y\,, \tag{8}$$

where $P(x,y,t)$ is the instantaneous pressure on the surface. The force $F_A(t)$ acting at point A is transformed into one force and two moments acting at node c, as illustrated in Fig. 2.

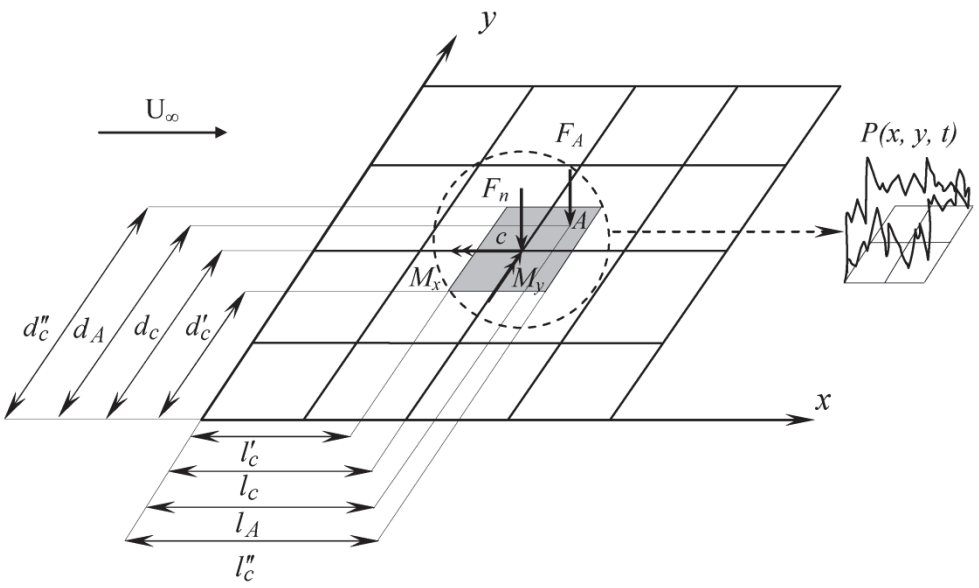

Fig. 2. Transformation of a continuous pressure field to a discrete force field and the equivalent discrete force field acting at node c. Pressure fluctuations are also illustrated laterally on the area surrounding node c.

The external load vector acting at a typical node c, $\mathbf{F}_c$ associated with the nodal displacements can be written in the following form:

$$\mathbf{F}_c(t)=\begin{Bmatrix}0\\0\\F_n\\M_y\\M_x\\0\end{Bmatrix}=\begin{Bmatrix}0\\0\\-\int_{d_i'}^{d_i''}\int_{l_i'}^{l_i''}P(x_i,y_i,t)\mathrm{d}x_i\,\mathrm{d}y_i\\-\int_{d_p'}^{d_p''}\int_{l_p'}^{l_p''}(x_p-l_p)P(x_p,y_p,t)\mathrm{d}x_p\,\mathrm{d}y_p\\-\int_{d_j'}^{d_j''}\int_{l_j'}^{l_j''}(y_j-d_j)P(x_j,y_j,t)\mathrm{d}x_j\,\mathrm{d}y_j\\0\end{Bmatrix}, \tag{9}$$

where F_n is the lateral force in the *z*-direction, M_x and M_y are the moments in the *x*- and *y*-directions acting at node *c*, respectively, and $l_i''=l_p''=l_j''=l_c''$, $l_i'=l_p'=l_j'=l_c'$, $d_i''=d_p''=d_j''=d_c''$, $d_i'=d_p'=d_j'=d_c'$, $l_p=l_c$ and $d_j=d_c$. This particular indicial notation is introduced for convenience in subsequent manipulations.

5. Response to an arbitrary random pressure field

If the pressure field is deterministic, the response as expressed by Eq. (7) is the solution. In the case of a random field; however, we must proceed differently. First we express the mean square of the response in terms of the spectral density of an arbitrary random pressure field. This is followed by presentation of the response to an arbitrary homogeneous random pressure field.

5.1. Mean square displacements in terms of the cross spectral density of an arbitrary random pressure

As mentioned earlier, a random process can only be described in statistical terms. Here, we assume that the random pressure is stationary in time and homogeneous in space, so the response can be expressed in terms of the cross-spectral density of the pressure. Assuming that we are dealing with an ergodic process and using the correlation theorem, the mean square displacement response at node g, $\overline{\boldsymbol{\delta}_g^2(x_g, y_g, t)}$ can be expressed as follows:

$$\overline{\boldsymbol{\delta}_g^2(x_g, y_g, t)} = \lim_{T\to\infty} \frac{1}{T} \int_0^{+\infty} \boldsymbol{\Delta}_g^*(x_g, y_g, f, T) \boldsymbol{\Delta}_g(x_g, y_g, f, T) \mathrm{d}f \,, \tag{10}$$

where $\boldsymbol{\Delta}$ and $\boldsymbol{\Delta}^*$ are the finite Fourier transforms of the nodal displacement and its complex conjugate, respectively, f is the frequency in Hz and T is the period. It should be stated that $\lim_{T\to\infty} \dfrac{\boldsymbol{\Delta}_g^* \boldsymbol{\Delta}_g}{T}$ is the one-sided auto spectral density of displacement.

Taking the Fourier transform of Eq. (6), we obtain the Fourier transform of the generalized coordinates as follows:

$$Q_r(f, T) = \frac{H_r(f) \boldsymbol{\Phi}_r^{\mathrm{T}} \mathbf{F}(f, T)}{4\pi^2 f_r^2 \bar{M}_r} \,, \tag{11}$$

where $\mathbf{F}(f, T)$ is the Fourier transform of the force vector and $H_r(f)$ is the frequency response function for the rth mode defined as follows:

$$H_r(f) = \left\{ 1 - \left(\frac{f}{f_r} \right)^2 + 2\mathrm{i}\zeta_r \left(\frac{f}{f_r} \right) \right\}^{-1} = \left| H_r(f) \right| \mathrm{e}^{-\mathrm{i}\theta_r(f)} \,, \tag{12}$$

where $|H_r(f)|$ and $\theta_r(f)$ are the magnification and phase factors, respectively, f is the forced frequency, f_r is the rth natural frequency and $\mathrm{i}^2 = -1$.

Substituting Eq. (11) into the Fourier transform of Eq. (7), the Fourier transform of the nodal displacement can be written as follows:

$$\mathbf{\Lambda}_g(f,T) = \sum_{r=1}^{N} \mathbf{\Phi}_{gr} \frac{|H_r(f)|\mathrm{e}^{-\mathrm{i}\theta_r(f)}}{4\pi^2 f_r^2 \bar{M}_r} \mathbf{\Phi}_r^{\mathrm{T}} \mathbf{F}(f,T). \tag{13}$$

Introducing Eq. (13) and its complex conjugate into Eq. (10), the mean square response at node g is obtained:

$$\overline{\boldsymbol{\delta}_g^2(x_g,y_g,t)} = \sum_{r=1}^{N}\sum_{s=1}^{N} \frac{\mathbf{\Phi}_{gr}(x_g,y_g)\mathbf{\Phi}_{gs}(x_g,y_g)}{(2\pi)^4 f_r^2 f_s^2 \bar{M}_r \bar{M}_s} \lim_{T\to\infty} \frac{1}{T} \int_0^{\infty} \mathrm{e}^{\mathrm{i}(\theta_S-\theta_r)} \left|H_r(f)\right| \left|H_s(f)\right| \{\mathbf{\Phi}\}_s^{\mathrm{T}} \mathbf{F}^*(f,T) \{\mathbf{\Phi}\}_r^{\mathrm{T}} \mathbf{F}(f,T) \mathrm{d}f, \tag{14}$$

where $\mathbf{\Phi}_{gr}$ and $\mathbf{\Phi}_{gs}$ are the rth and sth mode shapes at node g, $|H_r(f)|$ and $|H_s(f)|$ are the magnification factors for the rth and sth modes, θ_r and θ_s are the phase lags between the force and the response, and $\mathbf{F}(f,T)$ and $\mathbf{F}^*(f,T)$ are the Fourier transforms of the force vector and its complex conjugate, respectively.

For a lightly damped multi-degree-of-freedom system with well separated natural frequencies, the cross-product terms are much smaller than the self-product terms; therefore the contribution of the cross-product terms to the mean square displacement response can be ignored without significant loss of accuracy. Eq. (14) can then be rewritten as follows:

$$\overline{\boldsymbol{\delta}_g^2(x_g,y_g,t)} = \sum_{r=1}^{N} \frac{\mathbf{\Phi}_{gr}^2(x_g,y_g)}{16\pi^4 f_r^4 \bar{M}_r^2} \lim_{T\to\infty} \frac{1}{T} \int_0^{\infty} |H_r(f)|^2 \{\mathbf{\Phi}\}_r^{\mathrm{T}} \mathbf{F}(f,T) \{\mathbf{\Phi}\}_r^{\mathrm{T}} \mathbf{F}^*(f,T) \mathrm{d}f. \tag{15}$$

Note that loads acting at each node have three components: one lateral force and two moments about the in-plane directions. Therefore the cross spectral density of the force between any two nodes has nine terms.

We next define the one-sided cross spectral density of pressure:

$$G_{pp}(x_i, y_i, x_j, y_j, f) = \lim_{T\to\infty} \frac{1}{T}\left[P^*(x_i, y_i, f, T) P(x_j, y_j, f, T) \right], \tag{16}$$

where P and P^* are the Fourier transforms of the pressure and its complex conjugate, respectively.

Substituting the Fourier transform of the external force vector from Eq. (9) into Eq. (15), transforming the vector by summation and then introducing Eq. (16) into Eq. (15), the mean square response at node *g* is obtained as follows:

$$\overline{\boldsymbol{\delta}_g^2(x_g,y_g,t)}=\sum_{r=1}^{N}\frac{\boldsymbol{\Phi}_{gr}^2}{16\pi^4 f_r^4 \bar{M}_r^2}\int_0^{\infty}\left|H_r(f)\right|^2$$
$$\Big\{\sum_{i=1}^{n}\sum_{u=1}^{n}\Phi_{ir}\Phi_{ur}\int_{d_u'}^{d_u''}\int_{l_u'}^{l_u''}\int_{d_i'}^{d_i''}\int_{l_i'}^{l_i''}G_{pp}(x_i,y_i,x_u,y_u,f)\mathrm{d}x_i\mathrm{d}y_i\mathrm{d}x_u\mathrm{d}y_u+$$
$$\sum_{i=1}^{n}\sum_{v=1}^{n}\Phi_{ir}\Phi_{vr}\int_{d_v'}^{d_v''}\int_{l_v'}^{l_v''}\int_{d_i'}^{d_i''}\int_{l_i'}^{l_i''}(x_v-l_v)G_{pp}(x_i,y_i,x_v,y_v,f)\mathrm{d}x_i\mathrm{d}y_i\mathrm{d}x_v\mathrm{d}y_v+$$
$$\sum_{i=1}^{n}\sum_{k=1}^{n}\Phi_{ir}\Phi_{kr}\int_{d_k'}^{d_k''}\int_{l_k'}^{l_k''}\int_{d_i'}^{d_i''}\int_{l_i'}^{l_i''}(y_k-d_k)G_{pp}(x_i,y_i,x_k,y_k,f)\mathrm{d}x_i\mathrm{d}y_i\mathrm{d}x_k\mathrm{d}y_k+$$
$$\sum_{p=1}^{n}\sum_{u=1}^{n}\Phi_{pr}\Phi_{ur}\int_{d_u'}^{d_u''}\int_{l_u'}^{l_u''}\int_{d_p'}^{d_p''}\int_{l_p'}^{l_p''}(x_p-l_p)G_{pp}(x_p,y_p,x_u,y_u,f)\mathrm{d}x_p\mathrm{d}y_p\mathrm{d}x_u\mathrm{d}y_u+$$
$$\sum_{p=1}^{n}\sum_{v=1}^{n}\Phi_{pr}\Phi_{vr}\int_{d_v'}^{d_v''}\int_{l_v'}^{l_v''}\int_{d_p'}^{d_p''}\int_{l_p'}^{l_p''}(x_p-l_p)(x_v-l_v)G_{pp}(x_p,y_p,x_v,y_v,f)\mathrm{d}x_p\mathrm{d}y_p\mathrm{d}x_v\mathrm{d}y_v+$$
$$\sum_{p=1}^{n}\sum_{k=1}^{n}\Phi_{pr}\Phi_{kr}\int_{d_k'}^{d_k''}\int_{l_k'}^{l_k''}\int_{d_p'}^{d_p''}\int_{l_p'}^{l_p''}(x_p-l_p)(y_k-d_k)G_{pp}(x_p,y_p,x_k,y_k,f)\mathrm{d}x_p\mathrm{d}y_p\mathrm{d}x_k\mathrm{d}y_k+$$
$$\sum_{j=1}^{n}\sum_{u=1}^{n}\Phi_{jr}\Phi_{ur}\int_{d_u'}^{d_u''}\int_{l_u'}^{l_u''}\int_{d_j'}^{d_j''}\int_{l_j'}^{l_j''}(y_j-d_j)G_{pp}(x_j,y_j,x_u,y_u,f)\mathrm{d}x_j\mathrm{d}y_j\mathrm{d}x_u\mathrm{d}y_u+$$
$$\sum_{j=1}^{n}\sum_{v=1}^{n}\Phi_{jr}\Phi_{vr}\int_{d_v'}^{d_v''}\int_{l_v'}^{l_v''}\int_{d_j'}^{d_j''}\int_{l_j'}^{l_j''}(y_j-d_j)(x_v-l_v)G_{pp}(x_j,y_j,x_v,y_v,f)\mathrm{d}x_j\mathrm{d}y_j\mathrm{d}x_v\mathrm{d}y_v+$$
$$\sum_{j=1}^{n}\sum_{k=1}^{n}\Phi_{jr}\Phi_{kr}\int_{d_k'}^{d_k''}\int_{l_k'}^{l_k''}\int_{d_j'}^{d_j''}\int_{l_j'}^{l_j''}(y_j-d_j)(y_k-d_k)G_{pp}(x_j,y_j,x_k,y_k,f)\mathrm{d}x_j\mathrm{d}y_j\mathrm{d}x_k\mathrm{d}y_k\ \Big\}\mathrm{d}f,$$

(17)

where $\overline{\boldsymbol{\delta}_g^2}$ is the mean square displacement response of node g, $\boldsymbol{\Phi}_{gr}$ is the rth mode shape at node g, f_r is the rth natural frequency in Hz, f is the excitation frequency in Hz, $\bar{M}_r$ is the rth element of generalized mass matrix, $\left|H_r(f)\right|$ is the magnification factor for the rth mode, G_{pp} is the one-sided cross spectral density of pressure, N is the number of mode

shapes chosen for evaluation, n is the number of nodes, l_i and d_i are the coordinates of a typical node i in the x- and y-directions, respectively, l_i' and l_i'' are the limits of the area surrounding the node i in the x-direction, d_i' and d_i'' are the limits of the area surrounding the node i in the y-direction (see Fig. 2), and Φ_{ir}, Φ_{ur}, Φ_{pr}, Φ_{vr}, Φ_{jr}, Φ_{kr} represent the elements of the rth mode shape corresponding to the radial displacement, derivative of radial displacement with respect to x and derivative of radial displacement with respect to y, in respective pairs. We note that the indices i and u are associated with lateral forces, p and v with moments about y, and j and k with moments about x.

5.2. Power spectral density of displacements

As stated, one of the purposes of this study is to determine the total rms displacements. In addition, we are able to calculate PSD of displacements as a function of excitation frequency as follows:

$$G_{\boldsymbol{\delta}_g\boldsymbol{\delta}_g}(f)=\sum_{r=1}^{N}\frac{\boldsymbol{\Phi}_{gr}^2}{16\pi^4 f_r^4 \bar{M}_r^2}\left|H_r(f)\right|^2$$
$$\left\{\sum_{i=1}^{n}\sum_{u=1}^{n}\Phi_{ir}\Phi_{ur}\int_{d'_u}^{d''_u}\int_{l'_u}^{l''_u}\int_{d'_i}^{d''_i}\int_{l'_i}^{l''_i}G_{pp}(x_i,y_i,x_u,y_u,f)\mathrm{d}x_i\mathrm{d}y_i\mathrm{d}x_u\mathrm{d}y_u+\right.$$
$$\sum_{i=1}^{n}\sum_{v=1}^{n}\Phi_{ir}\Phi_{vr}\int_{d'_v}^{d''_v}\int_{l'_v}^{l''_v}\int_{d'_i}^{d''_i}\int_{l'_i}^{l''_i}(x_v-l_v)G_{pp}(x_i,y_i,x_v,y_v,f)\mathrm{d}x_i\mathrm{d}y_i\mathrm{d}x_v\mathrm{d}y_v+$$
$$\sum_{i=1}^{n}\sum_{k=1}^{n}\Phi_{ir}\Phi_{kr}\int_{d'_k}^{d''_k}\int_{l'_k}^{l''_k}\int_{d'_i}^{d''_i}\int_{l'_i}^{l''_i}(y_k-d_k)G_{pp}(x_i,y_i,x_k,y_k,f)\mathrm{d}x_i\mathrm{d}y_i\mathrm{d}x_k\mathrm{d}y_k+$$
$$\sum_{p=1}^{n}\sum_{u=1}^{n}\Phi_{pr}\Phi_{ur}\int_{d'_u}^{d''_u}\int_{l'_u}^{l''_u}\int_{d'_p}^{d''_p}\int_{l'_p}^{l''_p}(x_p-l_p)G_{pp}(x_p,y_p,x_u,y_u,f)\mathrm{d}x_p\mathrm{d}y_p\mathrm{d}x_u\mathrm{d}y_u+$$
$$\sum_{p=1}^{n}\sum_{v=1}^{n}\Phi_{pr}\Phi_{vr}\int_{d'_v}^{d''_v}\int_{l'_v}^{l''_v}\int_{d'_p}^{d''_p}\int_{l'_p}^{l''_p}(x_p-l_p)(x_v-l_v)G_{pp}(x_p,y_p,x_v,y_v,f)\mathrm{d}x_p\mathrm{d}y_p\mathrm{d}x_v\mathrm{d}y_v+$$
$$\sum_{p=1}^{n}\sum_{k=1}^{n}\Phi_{pr}\Phi_{kr}\int_{d'_k}^{d''_k}\int_{l'_k}^{l''_k}\int_{d'_p}^{d''_p}\int_{l'_p}^{l''_p}(x_p-l_p)(y_k-d_k)G_{pp}(x_p,y_p,x_k,y_k,f)\mathrm{d}x_p\mathrm{d}y_p\mathrm{d}x_k\mathrm{d}y_k+$$
$$\sum_{j=1}^{n}\sum_{u=1}^{n}\Phi_{jr}\Phi_{ur}\int_{d'_u}^{d''_u}\int_{l'_u}^{l''_u}\int_{d'_j}^{d''_j}\int_{l'_j}^{l''_j}(y_j-d_j)G_{pp}(x_j,y_j,x_u,y_u,f)\mathrm{d}x_j\mathrm{d}y_j\mathrm{d}x_u\mathrm{d}y_u+$$
$$\sum_{j=1}^{n}\sum_{v=1}^{n}\Phi_{jr}\Phi_{vr}\int_{d'_v}^{d''_v}\int_{l'_v}^{l''_v}\int_{d'_j}^{d''_j}\int_{l'_j}^{l''_j}(y_j-d_j)(x_v-l_v)G_{pp}(x_j,y_j,x_v,y_v,f)\mathrm{d}x_j\mathrm{d}y_j\mathrm{d}x_v\mathrm{d}y_v+$$
$$\left.\sum_{j=1}^{n}\sum_{k=1}^{n}\Phi_{jr}\Phi_{kr}\int_{d'_k}^{d''_k}\int_{l'_k}^{l''_k}\int_{d'_j}^{d''_j}\int_{l'_j}^{l''_j}(y_j-d_j)(y_k-d_k)G_{pp}(x_j,y_j,x_k,y_k,f)\mathrm{d}x_j\mathrm{d}y_j\mathrm{d}x_k\mathrm{d}y_k\right\},\tag{18}$$

where $G_{\boldsymbol{\delta}_g\boldsymbol{\delta}_g}(f)$ is the power spectral density of the nodal displacement at node g.

5.3. Mean square displacements in terms of the cross spectral density of an arbitrary homogeneous random pressure

The cross spectral density of a homogeneous pressure field can be expressed in terms of distances of separation $\xi_x = |x_i - x_u|$ and $\xi_y = |y_i - y_u|$ instead of the coordinates themselves. Therefore, the one-sided cross spectral density of the pressure can be written as

$$G_{pp}(\xi_x, \xi_y, f) = G_{pp}(x_i, y_i, x_u, y_u, f) = \lim_{T\to\infty} \frac{1}{T} P(x_i, y_i, f) P^*(x_u, y_u, f), \tag{19}$$

Thus all the components of the cross spectral density of the wall pressure in Eq. (17) can be expressed in terms of $G_{pp}(\xi_x, \xi_y, f)$.

The one-sided cross spectral density of the wall pressure can be described by

$$G_{pp}(\xi_x, \xi_y, f) = G_{pp}(f)\Psi(\xi_x, \xi_y, 0), \tag{20}$$

where $G_{pp}(f)$ is the one-sided power spectral density of the pressure and $\Psi(\xi_x, \xi_y, 0)$ is the spatial correlation function between two points at the wall with a spatial separation of ξ_x and ξ_y, streamwise and spanwise, respectively. These spatial separations should be determined experimentally. Eqs. (17), (19) and (20) together express the response of a thin plate subjected to an arbitrary homogeneous random pressure field.

6. Response to a subsonic boundary layer pressure field

In the preceding section, expressions for the response of a thin plate subjected to an arbitrary homogeneous random pressure field were obtained; however, the origin of the

pressure field was left undefined. A model of the cross spectral density of the fluctuating pressure field $G_{pp}(\xi_x, \xi_y, f)$ is needed as an input to the numerical prediction algorithm.

Here we consider the particular case where the pressure field arises from pressure fluctuations in the subsonic, turbulent boundary layer of a flowing fluid. In the turbulent flow boundary layer, pressure fluctuates randomly so it cannot be described deterministically. Hence statistical methods should be employed to find the pressure.

6.1. Dynamics effects of a flow

We have indicated [25] how the inertial effects of a quiescent fluid contained by a shell or a shell partially or completely submerged in a stationary fluid may be taken into account. The salient point is given here; the fluid pressure applied on the structure is determined by combining potential flow theory, Bernoulli's equation and an impermeability condition and is expressed as a function of the acceleration of the normal displacement ($\partial^2 W / \partial t^2$) of the shell. Consequently, it can be interpreted as the virtual added mass of the fluid. However, when the fluid is flowing the shell is subjected to additional terms such as centrifugal and Coriolis-type forces. The former is proportional to $U^2 \partial^2 W / \partial x^2$ and considered as the stiffness of the fluid and has a diminishing effect on the natural frequencies of the system. The latter is proportional to $2U \partial^2 W / \partial x \partial t$ and has a damping effect on vibration. The magnitude of these effects depends on the dimensionless flow velocity ($U[(1-\nu^2)\rho / E]^{1/2}$), where U is the mean flow velocity, ν is Poisson's ratio, ρ is the fluid density and E is Young's modulus. The effect of these forces can be neglected unless we are dealing with

very flexible shells, very heavy fluids, or very high velocities. In any case, for metal shells in the vicinity of fluid with flow velocity in the normal engineering range, damping and stiffness effects of the flow are negligible [13] and will not be taken into account in this paper. Therefore the effects of the flow on the shell can be considered the same as the effects of a stationary fluid in contact with the shell.

6.2. Statistical properties of fluctuating wall pressure in a turbulent boundary layer

6.2.1. Cross correlation function

Correlation decay in oblique directions, whether between points on the same plate or between points on different plates, is represented by the product of the lateral and longitudinal decay functions. This independent-planes model of the pressure field for oblique directions was first suggested by Corcos [1] based on existing measurements. White [26] showed that the approximate separability does not introduce significant error. This theory was justified analytically by Curling and Païdoussis for clusters of cylinders [14] and was experimentally verified by Bakewell [27] for a body of revolution in a water medium. The cross correlation function can be written as follows:

$$\Psi(\xi_x,\xi_y,0)=\Psi(\xi_x,0,0)\Psi(0,\xi_y,0), \tag{21}$$

where $\Psi(\xi_x,0,0)$ and $\Psi(0,\xi_y,0)$ are the streamwise and spanwise spatial correlation decay functions, respectively.

In the case of subsonic turbulent boundary-layer pressure fluctuations the longitudinal and lateral spatial correlation functions have been examined theoretically and experimentally by several investigators. For example, Clinch [28] measured the narrowband longitudinal and circumferential correlations in thin-walled pipes when influenced by the passage of fully developed turbulent water flow.

Bakewell obtained lateral and longitudinal correlations in a turbulent boundary layer for a body of revolution in a water medium [27] and compared the results with the data obtained in flat plate boundary layers by Bull [8] and Willmarth and Wooldridge [7,29], and with data from pipe flows which he generated himself [30]. The results showed that the statistical properties of fluctuating wall pressure in a turbulent boundary layer for a body of revolution were in good agreement with data obtained in flat plate boundary layers and also in pipe flows. This agreement was demonstrated for the spectral density and the lateral and longitudinal correlation functions [27]. Different empirical expressions for different structures have been suggested for longitudinal and lateral correlations; however, these expressions are approximately the same.

Corcos postulated that the longitudinal and lateral correlations may be presented as an exponentially decaying oscillating function in the flow direction and a simple exponentially decaying function in the cross-flow direction, respectively, as follows:

$$\Psi(\xi_x,0,0) = \mathrm{e}^{-\alpha_x 2\pi\left|S_{\xi x}\right|}\mathrm{e}^{\mathrm{i}2\pi S_{\xi x}}, \tag{22a}$$

$$\Psi(0,\xi_y,0) = \mathrm{e}^{-\alpha_y 2\pi\left|S_{\xi y}\right|}, \tag{22b}$$

where

$$S_{\xi x} = \frac{f \xi_x}{U_c}, \tag{22c}$$

$$S_{\xi y} = \frac{f \xi_y}{U_c}, \tag{22d}$$

α_x and α_y are empirically determined constants, $S_{\xi x}$ and $S_{\xi y}$ are the Strouhal numbers, f is the excitation frequency, ξ_x and ξ_y are the streamwise and spanwise distances of separation, respectively, and $\mathrm{i} = \sqrt{-1}$. The convection velocity U_c over smooth walls is assumed to be a constant given by $U_c = 0.6U_\infty$ [8] where U_∞ is the free stream velocity.

Blake recommends that $\alpha_x = 0.116$ and $\alpha_y = 0.7$ be used for smooth walls [9]. It is to be expected that these constants will be approximately the same for different fluids at the same Strouhal number, at least for those with a sufficiently high Reynolds number.

It should be noted that mean square response is a real value, so the real part of the cross spectral density of the wall pressure should be taken into consideration. Putting all of these together and substituting Eqs. (22a) and (22b) into Eqs. (20) and (21), the wall pressure cross spectral density ($G_{pp}(\xi_x, \xi_y, f)$) in a fully developed turbulent region can be written as follows:

$$G_{pp}(\xi_x, \xi_y, f) = G_{pp}(f)\, \mathrm{e}^{-\alpha_x 2\pi \left| S_{\xi x} \right|}\, \mathrm{e}^{-\alpha_y 2\pi \left| S_{\xi y} \right|} \cos(2\pi S_{\xi x}), \tag{23}$$

where $G_{pp}(f)$ is the one-sided power spectral density of the wall pressure, $S_{\xi x}$ and $S_{\xi y}$ are the Strouhal numbers, f is the frequency in Hz, and α_x and α_y are constants describing the spatial coherence of the wall pressure field in longitudinal and lateral directions, respectively (see Eq. (17)).

6.2.2. Wall pressure power spectral density

The most significant characteristic of turbulent flow is the power spectral density. Fluctuating wall pressure beneath a turbulent boundary layer for various velocities has been measured for different structures and the non-dimensional wall-pressure PSD as a function of Strouhal number has been proposed by several investigators. Measurements of wall fluctuation, auto- and cross spectral, have been made on the outside walls of cylinders with flow along the axis by Willmarth and Young [31]. The power spectral density of wall pressure fluctuations on smooth-walled pipe was measured by Clinch [32]. He illustrated the comparison between his results with those measured by Bakewell et al. [5] for subsonic airflow in a smooth-walled pipe. Good agreement was found except at low Strouhal numbers due to the effects of extraneous noise, which increased the measured power spectral density. The power spectral density of the turbulent wall pressure fluctuations on a body of revolution in a water medium was obtained by Bakewell [27] and the result was in good agreement with pressure data obtained on flat plates and in fully developed turbulent pipe flow. Willmarth and Wooldridge measured the power spectral density of fluctuating pressure at a wall beneath a thick turbulent boundary layer [7]. Bakewell et al. [5] obtained measurements of the mean square pressure per unit bandwidth, i.e. the one-sided power spectral density versus Strouhal number for airflow at different Reynolds numbers in a pipe. The best curve fit for these measurements was obtained by Lakis [13].

Although there are differences in investigation characteristics, namely pipe radius, velocity and even the geometry of structure, the general features and magnitude of the spectral density are similar. The general trends of wall-pressure PSD obtained by Bakewell

et al. in pipe airflow, by Clinch in pipe water flow, by Willmarth and Wooldridge over a flat plate boundary layer, and in a straight flow channel are similar as shown by Au-Yang [33]. Therefore, it seems that the proposed expression by Lakis is applicable to a thin plate as follows [13]:

$$G_{pp}(f) = k_2 \rho_f^2 \delta^* U_\infty^3 \, \mathrm{e}^{-k_1 \delta^* f / U_\infty}, \tag{24}$$

where $G_{pp}(f)$ is the one-sided power spectral density of the pressure, k_1=0.25, k_2=2×10^{-6}, ρ_f is the density of the fluid, f is the frequency in Hz, δ^* is the boundary layer displacement thickness and U_∞ is the free stream velocity. It should be emphasized that the power spectral density of the pressure in Eq. (24) and all its implications apply to excitation frequencies above $f\delta^*/U_\infty$ of the order 0.1 due to the absence of empirical data below that point [13].

The well-known Schlichting formula is used to estimate boundary layer thickness δ [34]:

$$\delta = 0.37 x (\mathrm{Re}_x)^{-0.2}, \tag{25}$$

where $\mathrm{Re}_x = U_\infty x / \nu$ is the Reynolds number at the distance from the leading edge of the plate, ν is the kinematic viscosity, x is the distance from the leading edge of the plate and U_∞ is the free stream velocity. The boundary layer displacement thickness δ^* is approximated as 0.125 times the boundary layer thickness δ over smooth walls.

6.3. Mean square response

Substituting the power spectral density of the pressure from Eq. (24) into Eq. (23) and then introducing the cross spectral density of the pressure into Eqs. (17) and (19) and taking integrations over surface and frequency, the mean square displacement response ($\boldsymbol{\delta}_g^2$) is obtained as follows:

$$\overline{\boldsymbol{\delta}_g^2(x_g,y_g,t)}=\sum_{r=1}^{N}\frac{\boldsymbol{\Phi}_{gr}^2}{16\pi^4 f_r^4 \bar{M}_r^2}\left[\begin{array}{l}\sum_{i=1}^{n}\sum_{u=1}^{n}\Phi_{ir}\Phi_{ur}\left|\Gamma_{iu}\right|+2\sum_{i=1}^{n}\sum_{v=1}^{n}\Phi_{ir}\Phi_{vr}\left|\Gamma_{iv}\right|+2\sum_{i=1}^{n}\sum_{k=1}^{n}\Phi_{ir}\Phi_{kr}\left|\Gamma_{ik}\right|+\\ 2\sum_{p=1}^{n}\sum_{k=1}^{n}\Phi_{pr}\Phi_{kr}\left|\Gamma_{pk}\right|+\sum_{p=1}^{n}\sum_{v=1}^{n}\Phi_{pr}\Phi_{vr}\left|\Gamma_{pv}\right|+\sum_{j=1}^{n}\sum_{k=1}^{n}\Phi_{jr}\Phi_{kr}\left|\Gamma_{jk}\right|\end{array}\right], \qquad (26)$$

where Φ_{ij}'s are the terms of the modal matrix, f_r is the *r*th natural frequency in Hz, $\bar{M}_r$ is the *r*th element of the generalized mass matrix and Γ's are complicated functions given in detail in the Appendix. If the total response is desired, the response must be summed over all significant modes of vibration.

7. Calculations and discussions

7.1. Computational method and computer program

To determine the response of a thin structure to a random pressure we must proceed as follows: (i) the structure must be divided into a sufficient number of finite elements; (ii) the mass and stiffness matrices for each finite element must be determined; (iii) the global mass and stiffness matrices must be constructed; (iv) the eigenvalues and eigenvectors must be

computed; and (v) the rms response must be calculated at each node.

We must proceed with Eq. (26) where a great deal of the computational task has already been carried out. An in-house program in FORTRAN language has been developed for carrying out the aforementioned steps and determining the response to turbulent boundary-layer pressure fields. The process is summarized by the flow chart given in Fig. 3.

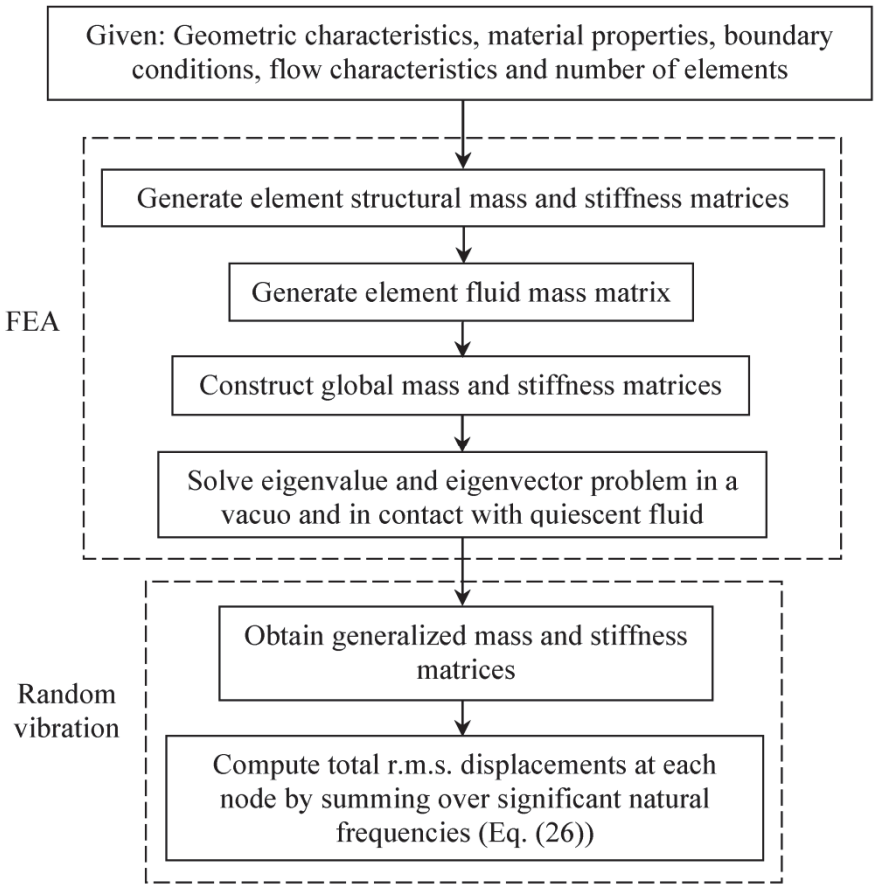

Fig. 3. Flow chart of the in-house program for calculation of rms displacement response.

The necessary time for calculation of the total rms displacement response for a plate composed of 100 elements is approximately 20 minutes. This corresponds to the case in

which numerous natural frequencies are utilized in the calculation of the total rms response. However, if only a few of the lowest natural frequencies are employed the total rms response can be calculated with an adequate degree of accuracy while computational costs can be considerably reduced. Moreover, the computer calculation includes determination of the total rms of all degrees of freedom at every node. A large amount of time may be saved if the response is not required at every node, or if only the total rms radial displacement is desired.

The present method and its associated computer program is capable of predicting the total rms response of a thin structure subjected to subsonic turbulent boundary layer pressure fluctuations with arbitrary boundary conditions. We are able to predict rms response at a given mode as well as total rms displacement over significant modes of vibration, which is the case in most applications.

7.2. Verification of the method

In order to check the validity of the method a long thin simply supported cylindrical shell having a length of 240 in, a radius of 3 in, and a thickness of 0.025 in, conveying water was studied. The material properties are: Young's modulus $E = 28.5\times10^{6}$ lb in^{-2}, Poisson's ratio $\nu = 0.305$, density $\rho = 0.749\times10^{-3}$ lb s^{2} in^{-4} and damping ratio $\zeta = 2\times10^{-2}$. This shell was first studied by Clinch both theoretically and experimentally [12]. He obtained the mean square radial displacement in the frequency range of 100-1000 Hz. Lakis and Païdoussis then analyzed the cylindrical shell using cylindrical finite elements [13].

They developed a method to obtain the root mean square displacements associated with each circumferential wavenumber. Natural frequencies of the shell were calculated first and it was found that many of these natural frequencies were below 100 Hz. This indicates that the high frequency response as measured by Clinch will differ significantly from the total response. Lakis and Païdoussis obtained the high frequency response of the radial displacement by taking into account only the modes whose natural frequencies were in the range of 93-1000 Hz. Good agreement between their theoretical results and Clinch's experimental results was found and the results lend confidence that the values of the overall response of the shell obtained by them may also be reliable. They also calculated total response of the radial displacement of the axial mid-point by considering all frequency components. This was accomplished by summing the results with circumferential wavenumbers 2-6 at the flow velocities 248 and 520 in s^{-1} (see Table 1 and Fig. 9 in Ref. [13]). The total root mean square response of radial displacement was found to be much higher than the response in the frequency range of 93-1000 Hz. As expected, the contribution to the total response increases substantially with decreasing frequency.

To the author's knowledge, there is no reference in the literature for the total rms displacement of a plate or an open curved structure subjected to a random pressure field arising from a boundary layer induced by turbulent flow. Therefore, in order to verify our method at least qualitatively, the aforementioned shell was analyzed. First, natural frequencies were calculated using our method and we observed that there are frequencies lower than those associated with circumferential wavenumber n=2. These frequencies are associated with a beam-like mode of the cylinder (i.e. n=1), which was not taken into account in Lakis' work. It should be noted that in the case of a long slender cylinder some

frequencies associated with the beam-like mode are the lowest natural frequencies of the system. The total rms radial displacement at the axial mid-point of a simply supported cylindrical shell was calculated for centerline velocities (U_{cl}) 248 and 520 in s^{-1} using our method developed in this work. The results are tabulated in Table 1 and compared with those obtained by Lakis.

Table 1

Comparison of the total rms radial displacement (W) at the axial-midpoint of a simply supported cylinder subjected to fully developed turbulent internal flow

	Total root mean square radial displacement (in)	
U_{cl} (in s^{-1})	Lakis' theory, by summation over n=2-6 [13]	Present method
248	1.9238E-04	3.1146E-04
520	1.4389E-03	1.8627E-03

As seen in Table 1, the responses calculated by our method using flat shell elements are of the same order but higher than those obtained by Lakis and Païdoussis. The total responses obtained by Lakis were calculated by summing the results over circumferential modes from n=2 to 6 only and the responses corresponding to the beam-like mode have not been taken into account. In our method, response calculation was carried out for all frequencies regardless of circumferential or axial modes, which could justify the higher

values. This discrepancy is attributed to the lower natural frequencies of the system that have been included in our method. It should be noted that because of the mixed combination of the low and high frequencies associated with the beam-like mode, we were not able to remove these frequencies from those calculated in our program. The power spectral density of the radial displacement at the axial-midpoint of the abovementioned cylindrical shell for a centerline velocity of 248 in s^{-1} and a damping ratio of 0.02 is illustrated in Fig. 4. It clearly demonstrates the significant contribution of the lower natural frequencies to the PSD of response.

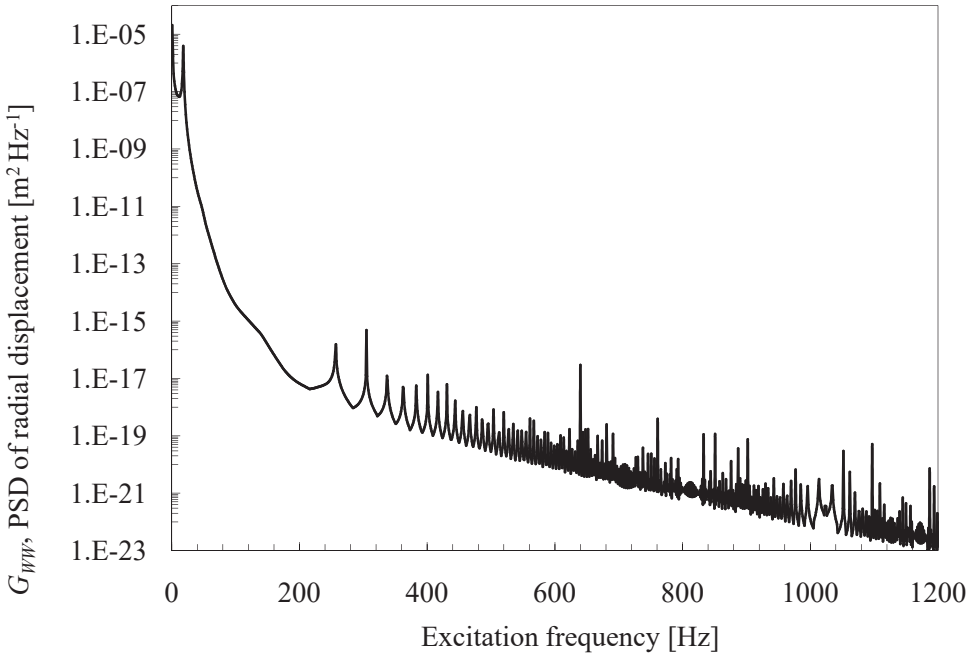

Fig. 4. Power spectral density of radial displacement (G_{WW}) at the axial-midpoint of a simply supported cylindrical shell subjected to fully developed turbulent internal flow versus excitation frequency for a centerline velocity of 248 in s^{-1} and a damping ratio of 0.02.

7.3. Response of a plate subjected to a turbulent boundary-layer-induced random pressure field

The geometry and material properties of the plate chosen herein are taken from reference [35]. The steel plate has a length of 0.655 m, a width of 0.20165 m and a thickness of 0.00936 m. The material properties are: Young's modulus $E = 207\times10^9$ Pa, Poisson's ratio $\nu = 0.3$ and density $\rho = 7850$ kg m^{-3}.

The plate is discretized into 10×10 flat rectangular elements. Further refining of the mesh beyond this did not influence the free vibration characteristics of the system. The same mesh has been used for calculation of the random response. Table 2 shows the convergence of the natural frequencies of a plate simply supported at its short sides subjected to quiescent water from one side where the height of fluid is more than 50 percent of the length of the plate. It is observed that the mesh refinement has no effect on the natural frequencies of the system.

Natural frequencies of the abovementioned SFSF plate subjected to quiescent water from one side were calculated numerically using a flat rectangular element and the method outlined in Refs. [24,25]. The first few natural frequencies of the aforementioned system compared well with corresponding analytical values in Ref. [35] and are listed in Table 3. For the sake of brevity we did not tabulate the natural frequencies of the plate under different boundary conditions wetted from one or both sides using our method. However, in all cases good agreement was found between our numerical results and those obtained in Ref. [35].

Table 2

Convergence of natural frequencies of an SFSF plate subjected to stationary water from one side

Coupled natural frequency (Hz)		Discrepancy (%)
Mesh 10×10	Mesh 20×20	
37.68	37.68	0.00
152.10	152.08	0.01
171.03	171.03	0.00
344.96	344.78	0.05
367.39	367.38	0.00
609.41	609.30	0.02
617.20	616.21	0.16
911.05	910.35	0.08

Table 3

Comparison of the natural frequencies of an SFSF plate subjected to stationary water from one side

Coupled natural frequency (Hz)		Discrepancy (%)
Haddara & Cao (analytic) [35]	Present method	
34.81	37.68	7.62
145.66	152.10	4.23
NA	171.03	NA
348.30	344.96	0.97
NA	367.39	NA

The same plate was used and we obtained its response to turbulent boundary layer pressure fluctuations under different boundary conditions. It should be mentioned that the root mean square response has not been studied in Ref. [35]. Here, the total rms displacement responses of the plate were obtained by summation over all significant modes of vibration (see Eq. (26)) at all nodes and then the maximum total rms response of the plate was calculated. Two sets of flow (i.e. fluid flowing over the plate and fluid flowing on both sides of the plate) and different boundary conditions of the plate were considered in this work. The effect of flow direction on the response was also investigated. The power spectral densities of the in-plane and out-of plane displacements of an SFSF plate were studied. In order to check the role of damping as revealed in Eq. (12), two damping ratios were considered in the calculation of the response.

7.3.1. SFSF plate

7.3.1.1. Response of an SFSF plate subjected to turbulent flow along its long sides from one side and both sides, respectively (Figs. 5-7, and Tables 4-6)

The first case study is a plate which is simply supported at its short sides, over which water is flowing along the long side of the plate at a height more than 50 percent of the length of the plate. Based on previous analyses [24,25] the natural frequencies of the plate in contact with quiescent water are calculated (see Table 3). As stated in Section 6.1, solely the inertial effect of the fluid is taken into account in this work. It is worth mentioning that when the fluid height exceeds 50 percent of the length of the plate the boundary conditions

of the fluid at the extremity and the height of the fluid are of no importance when considering natural frequency changes [25].

The variation of the rms radial displacements with natural frequency for the aforementioned SFSF plate subjected to turbulent boundary-layer-induced random pressure fluctuations from one side is presented in Table 4. The results are calculated for a free stream velocity of 25 m s^{-1} and a damping ratio of 0.001 at the node at which the maximum total rms radial displacement was observed. The natural frequencies of the plate in a vacuum and in contact with stationary fluid from one side are listed in Table 4.

As expected the natural frequencies of the plate subjected to fluid at rest are lower than those of the plate in a vacuum. Table 4 indicates that the lower natural frequencies contribute significantly to the response and as natural frequency increases the rms response becomes insignificant quickly. It can be clearly seen from Eq. (26) that the response is inversely proportional to the square of the natural frequency. This therefore indicates that the first six natural frequencies suffice to calculate the total response for the plate studied here.

Table 4

Variation of the maximum rms radial displacement with natural frequency for an SFSF plate subjected to turbulent boundary-layer-induced random pressure fluctuations from one side where water is flowing along the long side of the plate for U_∞= 25 m s^{-1} and $\zeta = 10^{-3}$

Natural frequency of an SFSF plate in a vacuum (Hz)	Natural frequency of an SFSF plate in contact with stationary fluid from one side (Hz)	r.m.s. radial displacement (m)
51.04	37.68	0.1519E-03
206.03	152.10	0.1202E-05
231.68	171.03	0.3169E-05
467.28	344.96	0.9016E-07
497.66	367.39	0.1377E-06
825.50	609.41	0.2099E-07
836.05	617.20	0.1855E-07
1234.10	911.05	0.7687E-08

As mentioned in Section 7.3, refining of the mesh did not influence the natural frequencies of the plate in contact with fluid (see Table 2). However, mesh refinement may yield slightly different rms displacement response. The effect of mesh refinement on the maximum total rms radial displacement of the SFSF plate subjected to turbulent boundary layer from one side where fluid is flowing along the long side of the plate for U_∞= 25 m s^{-1} and $\zeta = 0.001$ is presented in Table 5. It is observed that the mesh refinement has almost no considerable effect on the response and the total rms radial displacement differs only about 4 percent but the calculation is very costly and time consuming. Therefore the mesh of 10×10 flat rectangular elements is used for the calculation hereafter.

Table 5

Comparison of the maximum total rms radial displacement of an SFSF plate subjected to turbulent boundary-layer-induced random pressure fluctuations from one side where water is flowing along the long side of the plate for U_∞= 25 m s^{-1} and $\zeta = 10^{-3}$

Mesh size	Max. total r.m.s. radial displacement (m)	CPU time
10×10	0.1520E-03	20 min
20×20	0.1596E-03	30 h

The maximum total rms displacement responses of the SFSF plate over which water is flowing along its long sides as a function of free stream velocity in the range of 5-30 m s^{-1} and for different damping ratios, namely $\zeta = 10^{-2}$ and 10^{-3} are shown in Fig. 5. It is assumed that the turbulent boundary layer is fully developed over the entire plate. The results plotted in Fig. 5 reveal that the total rms displacements are inversely proportional to the damping ratio and directly proportional to the free stream velocity. In order to demonstrate the behavior of rms responses, the maximum total rms membrane displacements (U and V) are also plotted in Fig. 5. As anticipated, the membrane displacements of the plate are minimal. The maximum total rms radial displacement is displayed on a secondary axis due to its higher value. The effects of the membrane responses are minimal for all boundary conditions of the plate. For this reason further studies will only consider radial displacement of the plate.

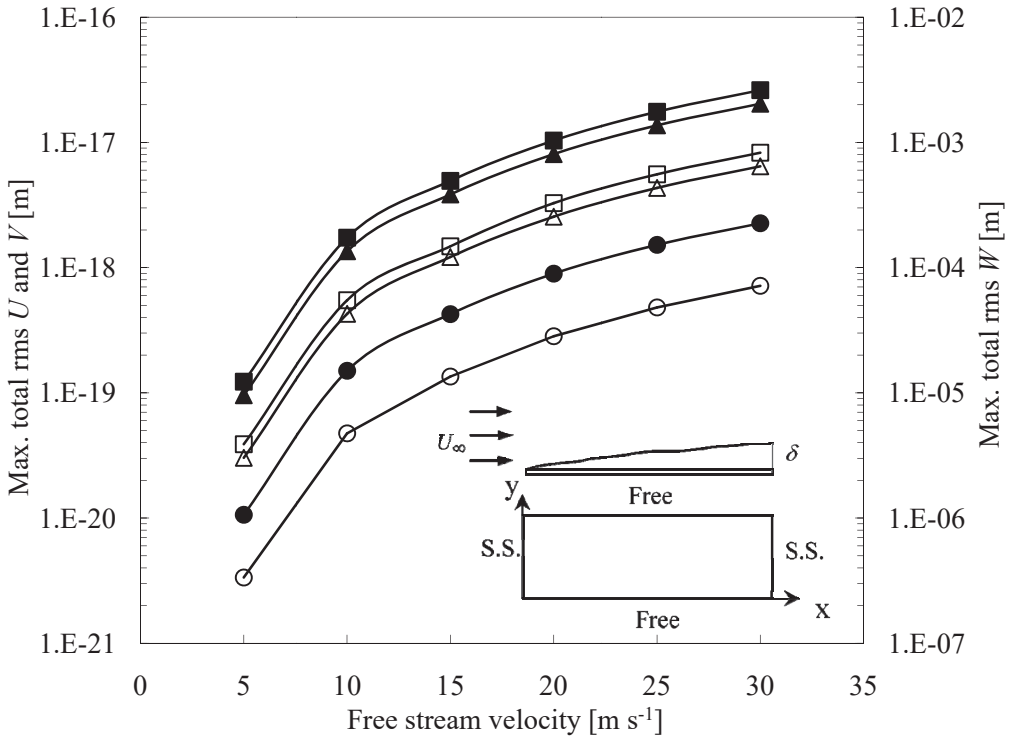

Fig. 5. Maximum total rms displacement responses (U, V and W) versus free stream velocity and damping ratio (ζ) for an SFSF plate subjected to fully developed turbulent flow from one side, where water is flowing along the long side of the plate: —■— U, ζ=10^{-3}, —▲— V, ζ=10^{-3}, —●— W, ζ=10^{-3}, —□— U, ζ=10^{-2}, —△— V, ζ=10^{-2}, —○— W, ζ=10^{-2}. The maximum total rms radial displacement (W) is plotted on secondary axis due to its higher value in comparison to the minimal rms membrane displacements (U and V). It is observed that the total rms displacements are inversely proportional to damping ratio and directly proportional to free stream velocity.

The power spectral density of the radial displacement (G_{WW}) of the aforementioned SFSF plate subjected to fully developed turbulent flow from one side where flow is along its long sides is plotted against excitation frequency in Fig. 6. The PSD of the radial

displacement in Fig. 6 is calculated for a free stream velocity of 30 m s^{-1} and a damping ratio of 0.001 at the node at which the maximum total rms radial displacement was obtained (see also Fig. 5). As expected, it shows dominant peaks with coupled natural frequency values corresponding to those given in Table 3.

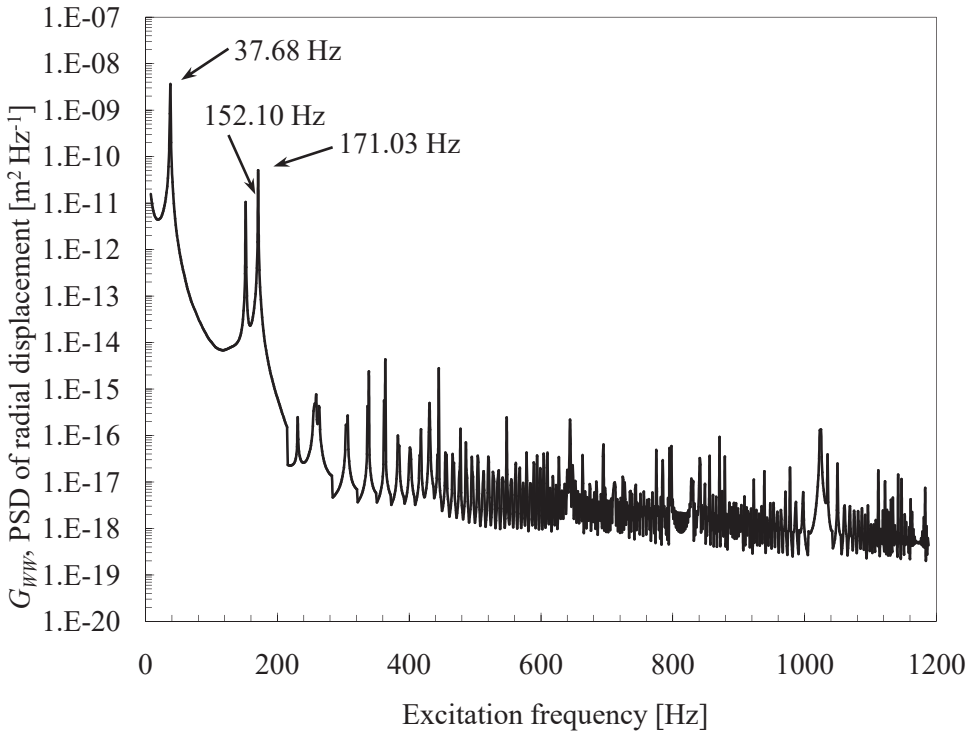

Fig. 6. Power spectral density of radial displacement (G_{WW}) of an SFSF plate subjected to fully developed turbulent flow from one side where flow is along its long sides against excitation frequency. The PSD of the radial displacement is calculated at the node at which the maximum total rms radial displacement response was obtained for a free stream velocity of 30 m s^{-1} and a damping ratio of 0.001 (see also Fig. 5). The major peaks demonstrate the natural frequencies of the system given in Table 2. It is observed that lower natural frequencies contribute significantly to the response.

Also as expected, the PSDs of the in-plane displacements (G_{UU} and G_{VV}) are minimal; however, for the sake of demonstration the power spectral densities of the in-plane displacements of the aforementioned SFSF plate subjected to fully developed turbulent flow from one side where flow is along its long sides are illustrated against excitation frequency in Fig. 7. The PSDs of the in-plane displacements in Fig. 7 are calculated for a free stream velocity of 30 m s^{-1} and a damping ratio of 0.001 at the node at which the maximum total rms radial displacement response was obtained. The same major peaks as those in Fig. 6 are observed representing the natural frequencies of the system. It is observed that the lower natural frequencies contribute greatly to the PSD of response.

The maximum total rms radial displacement of the SFSF plate with a damping ratio of $\zeta=10^{-2}$ subjected to fully developed turbulent flow from both sides was calculated for the case where water is flowing along the long sides of the plate. The results are tabulated in Table 6 for different free stream velocities and compared with those with flow on one side of the plate. As anticipated, the response of the plate wetted on both sides is higher than the response of the plate over which water is flowing due to its lower natural frequencies and larger virtual added mass [25].

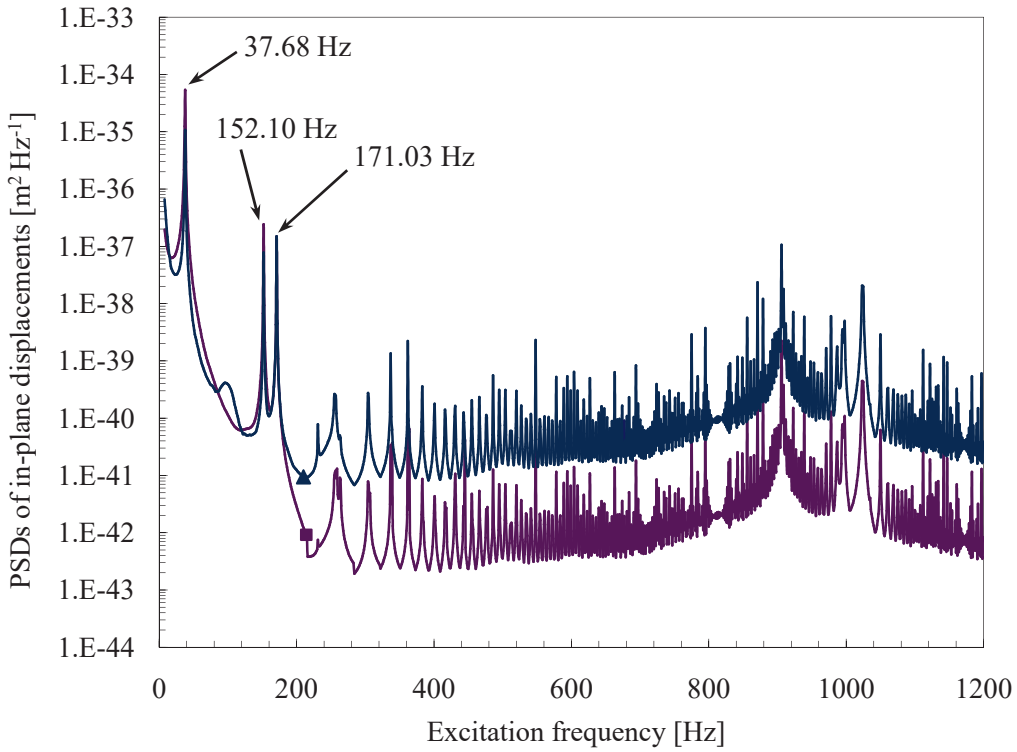

Fig. 7. Power spectral densities of in-plane displacements of an SFSF plate subjected to fully developed turbulent flow from one side where flow is along its long sides versus excitation frequency. The PSDs are calculated for a free stream velocity of 30 m s^{-1} and a damping ratio of 0.001 at the node at which the maximum total rms radial displacement response was obtained: —■— PSD of membrane displacement in the *x*-direction (G_{UU}), —▲— PSD of membrane displacement in the *y*-direction (G_{VV}). The PSDs of the in-plane displacements are minimal; however, for the sake of demonstrating the behavior, they are illustrated. The same major peaks as those in Fig. 6 are observed representing the natural frequencies of the system.

Table 6

Comparison of the maximum total rms radial displacement of an SFSF plate with a damping ratio of $\zeta = 10^{-2}$ subjected to fully developed turbulent flow from one and both sides for different free stream velocities, where water is flowing along the long side of the plate

U_∞ (m s^{-1})	Max. total r.m.s. radial displacement of a plate wetted on one side (m)	Max. total r.m.s. radial displacement of a plate wetted on both sides (m)
5	3.3552E-07	5.8416E-07
10	4.7501E-06	5.6450E-06
15	1.3484E-05	1.5456E-05
20	2.8316E-05	3.0860E-05
25	4.8085E-05	5.0640E-05
30	7.1533E-05	7.6949E-05

7.3.1.2. Effects of flow direction on rms radial displacement response (W) of an SFSF plate (Figs. 8 and 9)

The effects of flow direction on total rms radial displacement of an SFSF plate with water flowing on one or both sides were studied. Fig. 8 shows the maximum total rms radial displacement versus free stream velocity and damping ratio for the same SFSF plate studied earlier (see Fig. 5) but with water flowing over its short side. The results are also compared with those for the case of turbulent flow along the long side of the plate. It is observed that the rms radial displacements for the case of flow along the long side of the

plate is higher than those obtained for flow along the short side of the plate, except for the free stream velocity U_∞=5 m s^{-1}.

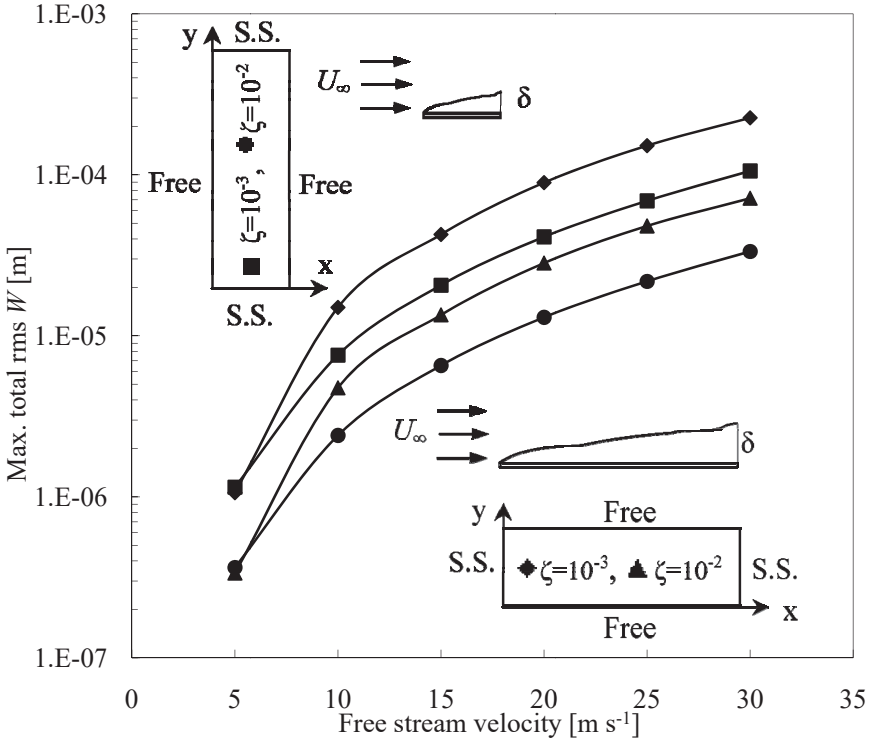

Fig. 8. Comparison of the effect of flow direction on the maximum total rms radial displacement of an SFSF plate subjected to fully developed turbulent flow from one side: —◆— flow along the long side of the SFSF plate with ζ=10^{-3}, —■— flow along the short side of the SFSF plate with ζ=10^{-3}, —▲— flow along the long side of the SFSF plate with ζ=10^{-2}, —●— flow along the short side of the SFSF plate with ζ=10^{-2}. Here, the maximum total rms radial displacements are illustrated against free stream velocity for different damping ratios. It is observed that the response for the case of flow along the long side of the plate is higher than that for the flow along the short side of the plate except for free stream velocity 5 m s^{-1}.

The maximum total rms radial displacement versus free stream velocity and damping ratio for an SFSF plate subjected to turbulent flow from both sides, where water is flowing along the short side of the plate is depicted in Fig. 9 and compared with the results where flow is along the long side of the plate. Contrary to Fig. 8, it is observed from Fig. 9 that flow direction has almost no effect on the response of the SFSF plate subjected to turbulent flow from both sides for a given velocity and damping ratio.

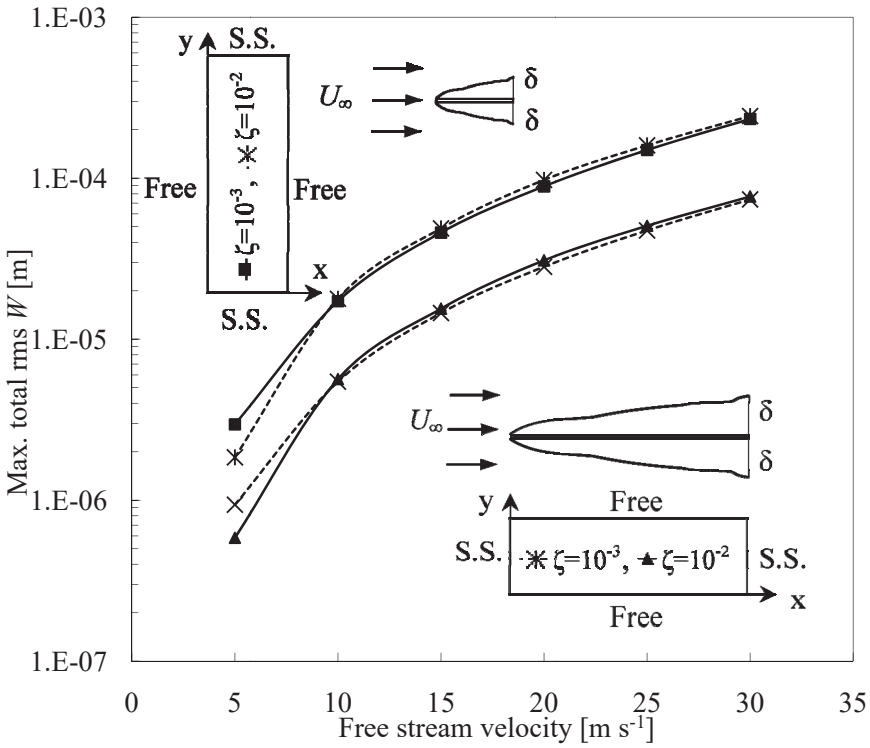

Fig. 9. Comparison of the effect of flow direction on the maximum total rms radial displacement of an SFSF plate subjected to fully developed turbulent flow from both sides: ··✳·· flow along the long side of the SFSF plate with $\zeta=10^{-3}$, —■— flow along the short side of the SFSF plate with $\zeta=10^{-3}$, —▲— flow along the long side of the SFSF plate with $\zeta=10^{-2}$, ··✳·· flow along the short side of the SFSF plate with $\zeta=10^{-2}$. The maximum total rms radial displacements are plotted against free stream velocity for different damping ratios, depicting that the response is relatively insensitive to flow direction.

7.3.2. Effects of flow direction on rms radial displacement (W) of a CFCF plate (Fig. 10)

The second case study is a plate which is clamped at its short sides subjected to fully developed turbulent flow from one side. In Fig. 10 the effect of flow direction on the

maximum total rms radial displacement is compared for two cases: water flowing over the short side of the CFCF plate and water flowing over the long side of the CFCF plate. The maximum total rms radial responses of the CFCF plate with different damping ratios as a function of free stream velocity are also seen in Fig. 10.

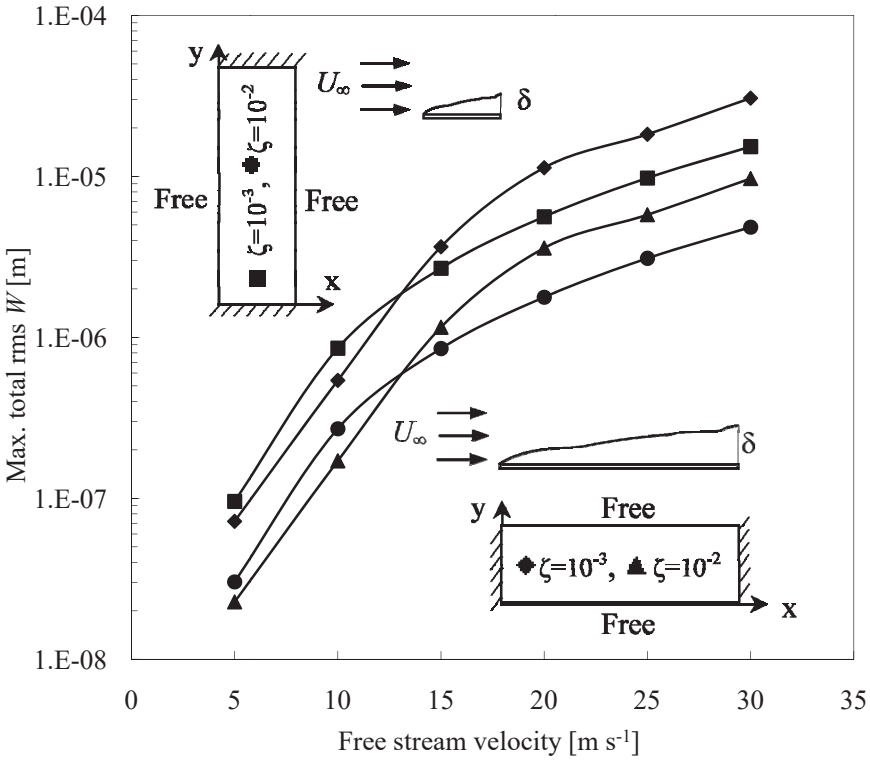

Fig. 10. Comparison of the effect of flow direction on the maximum total rms radial displacement of a CFCF plate subjected to fully developed turbulent flow from one side: —◆— flow along the long side of the CFCF plate with $\zeta=10^{-3}$, —■— flow along the short side of the CFCF plate with $\zeta=10^{-3}$, —▲— flow along the long side of the CFCF plate with $\zeta=10^{-2}$, —●— flow along the short side of the CFCF plate with $\zeta=10^{-2}$. The response is illustrated versus free stream velocity for different damping ratios. It is seen that the response for the case of flow along the long side of the plate is higher than that for the flow along the short side of the plate except for free stream velocities 5 and 10 m s^{-1}.

We observed that the maximum total rms radial response for the case of water flowing along the long side of the plate was lower than that obtained for the case of water flowing along the short side for free stream velocities 5 and 10 m s^{-1} and all damping ratios. On the other hand, the inverse behavior was observed for higher free stream velocities and all damping ratios.

As expected, the maximum total rms radial displacement is lower for the case of a CFCF plate than that obtained for an SFSF plate. This can be seen by comparing Figs. 8 and 10.

7.3.3. Effects of flow direction on rms radial displacement of a CFFF plate (Fig. 11)

A plate which is clamped at one short side subjected to fully developed turbulent flow from one side was investigated as the last case study. Fig. 11 illustrates the maximum total rms radial displacement versus free stream velocity and damping ratio for the aforementioned CFFF plate where water is flowing over its short side.

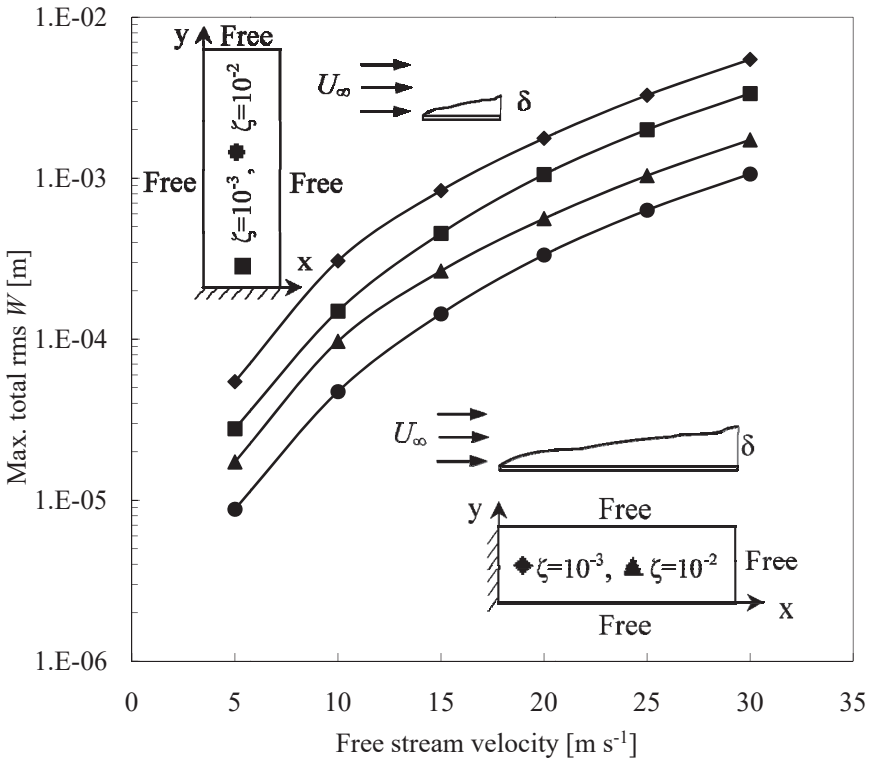

Fig. 11. Comparison of the effect of flow direction on the maximum total rms radial displacement of a CFFF plate subjected to fully developed turbulent flow from one side: —◆— flow along the long side of the CFFF plate with $\zeta=10^{-3}$, —■— flow along the short side of the CFFF plate with $\zeta=10^{-3}$, —▲— flow along the long side of the CFFF plate with $\zeta=10^{-2}$, —●— flow along the short side of the CFFF plate with $\zeta=10^{-2}$. The response is illustrated versus free stream velocity for different damping ratios. It shows that the response for the case of flow along the long side of the plate is higher than that for the flow along the short side of the plate for a given velocity and damping ratio.

The results are compared with those of an identically supported plate with turbulent flow along the long side. It was observed that the maximum total rms radial response for the case of water flowing along the long side of the plate is higher than that obtained for the case of

water flowing along the short side for all velocities and damping ratios. The effect of flow direction on the maximum total rms radial displacement versus free stream velocity and damping ratio for a CFFF plate subjected to turbulent flow from both sides shows the same behavior; however, for the sake of brevity this case has not been plotted. It should be noted that in all the aforementioned cases the same behavior was observed i.e. the total rms radial displacement is inversely proportional to the damping ratio and directly proportional to the free stream velocity.

8. Conclusion

In this paper we have introduced a method capable of predicting the total rms displacement response of a thin structure to an arbitrary random pressure field. The method was then specialized for application to the case where the pressure field originates from a turbulent boundary layer of a subsonic flow. This work is based on a previously developed method to obtain the dynamic behavior of thin structures in contact with fluid. This method uses a combination of classic thin shell theory and finite element analysis in which the finite elements are flat rectangular elements with six degrees of freedom per node, representing the in-plane and out-of-plane displacements and their spatial derivatives. Since the transverse displacement function is derived from thin plate theory this method may be easily adapted to take hydrodynamic effects into account. This method is also capable of calculating both high and low frequencies with high accuracy. This capability is normally of little interest in free vibration analysis but it is of great importance for determining the response of structures subjected to random pressure fields such as those generated by

turbulent flow. Wetted natural frequencies and mode shapes in a vacuum obtained using a previously developed method by the authors are incorporated into the calculation of random response. A random pressure field is estimated at each node of the finite element. Description of the turbulent pressure field is based on the Corcos formulation for the cross spectral density of pressure fluctuations. Root mean square displacement was found in terms of the cross spectral density of the pressure. A numerical approach is proposed to obtain the magnitude of the random response. Exact integration over surface and frequency leads to an expression for the response in terms of the wetted natural frequency of the system, undamped mode shapes, generalized mass matrix and other characteristics of the structure and flow.

An in-house program was developed to calculate the root mean square displacement response of a thin structure to random vibration due to the turbulent boundary layer of subsonic flow. The total rms displacement response was obtained by summation over all significant modes of vibration. To the author's knowledge, there is no reference in the literature for the total rms displacement of a plate or an open curved structure subjected to such random pressure. Therefore, in order to validate our method a cylindrical shell was analyzed and the total rms radial displacement was predicted and compared with that obtained by Lakis and Païdoussis. Although different expressions for correlations were adapted in the proposed method and in Lakis' work, good agreement was found. Since Lakis validated his results using Clinch's experimental measurements, this result shows that our method is sound.

The total root mean square displacement of a thin plate under various boundary conditions (i.e. SFSF, CFCF and CFFF) subjected to a boundary-layer-induced random

pressure field was studied and subsequently the maximum total rms displacement of the plate was predicted. The maximum total rms radial displacement responses as a function of free stream velocity for each set of flow and a given damping ratio were plotted for different boundary conditions of the plate. It was observed that they all have the same trend and the most sensitive case is the CFFF plate with higher magnitude.

The effect of flow direction on the response was also investigated. The effects of turbulent flow from one side and both sides of an SFSF plate on the rms radial displacement were investigated and higher responses in the case of the plate submerged in flow were obtained due to lower natural frequencies and larger virtual added mass, as expected. In all case studies it was observed that the maximum total rms displacement is directly proportional to free stream velocity and inversely proportional to the damping ratio. For each case study the same shift in response was observed as the damping ratio changed through all velocities. It is noted that the maximum total rms displacements are small for the set of calculations. Such small amplitudes are mainly of concern for fatigue considerations and must be below acceptable levels.

Furthermore, our method is capable of predicting the power spectral density of the displacement. The power spectral densities of the membrane and radial displacements of an SFSF plate subjected to fully developed turbulent flow from one side where flow is along the long sides of the plate versus excitation frequency were plotted. The spectrum shows the dominant peaks representing the coupled natural frequencies of the system. It was observed that the lower natural frequencies contribute significantly to the PSD of response.

This method can be applied to investigate parallel plates or a system of plates subjected to a fully developed turbulent random pressure field. As a future study, this work could be

extended to analyze three-dimensional thin curved structures subjected to a turbulent boundary layer random pressure field using a flat shell finite element with five degrees of freedom per node [25]. The same random vibration method is applicable and statistical properties such as power spectral density of pressure and correlations are more or less the same for different structures. Thin curved structures with discontinuities in thickness and material properties under different boundary conditions subjected to various boundary conditions of fluid can also be tackled.

Appendix A. Integration of lateral and longitudinal correlations

A.1. Integration of the longitudinal correlations in the x-direction

Substituting Eqs. (22a) and (22c) into Eqs. (21), (20) and (19) and then introducing the result into Eq. (17) and integrating over x to eliminate the space variable leads to expressions for the longitudinal correlations as follows:

$$\int_{l_i'}^{l_i''}\int_{l_u'}^{l_u''}\Psi(\xi_x,0,0)\mathrm{d}x_i\mathrm{d}x_u=\int_{l_i'}^{l_i''}\int_{l_u'}^{l_u''}\mathrm{e}^{-B|x_i-x_u|f}\cos\left(A(x_i-x_u)f\right)\mathrm{d}x_i\mathrm{d}x_u=$$

$$\frac{1}{f^2(A^2+B^2)^2}\begin{bmatrix}(B^2-A^2)\mathrm{e}^{-B|l_i'-l_u'|f}\cos\left(A(l_i'-l_u')f\right)\\-2AB\mathrm{e}^{-B|l_i'-l_u'|f}\sin\left(A(l_i'-l_u')f\right)\\-(B^2-A^2)\mathrm{e}^{-B|l_i'-l_u''|f}\cos\left(A(l_i'-l_u'')f\right)\\+2AB\mathrm{e}^{-B|l_i'-l_u''|f}\sin\left(A(l_i'-l_u'')f\right)\\-(B^2-A^2)\mathrm{e}^{-B|l_i''-l_u'|f}\cos\left(A(l_i''-l_u')f\right)\\+2AB\mathrm{e}^{-B|l_i''-l_u'|f}\sin\left(A(l_i''-l_u')f\right)\\+(B^2-A^2)\mathrm{e}^{-B|l_i''-l_u''|f}\cos\left(A(l_i''-l_u'')f\right)\\-2AB\mathrm{e}^{-B|l_i''-l_u''|f}\sin\left(A(l_i''-l_u'')f\right)\end{bmatrix}\tag{A.1a}$$

$$\int_{l_i'}^{l_i''}\int_{l_v'}^{l_v''}(x_v-l_v)\Psi(\xi_x,0,0)\mathrm{d}x_i\mathrm{d}x_v=\int_{l_i'}^{l_i''}\int_{l_v'}^{l_v''}(x_v-l_v)\mathrm{e}^{-B|x_i-x_v|f}\cos\left(A(x_i-x_v)f\right)\mathrm{d}x_i\mathrm{d}x_v=$$

$$\frac{1}{f^3(A^2+B^2)^3}\begin{bmatrix}(B^3-3A^2B)\mathrm{e}^{-B|l_i'-l_v'|f}\cos\left(A|l_i'-l_v'|f\right)\\+(A^3-3AB^2)\mathrm{e}^{-B|l_i'-l_v'|f}\sin\left(A|l_i'-l_v'|f\right)\\+(B^3-3A^2B)\mathrm{e}^{-B|l_i''-l_v''|f}\cos\left(A|l_i''-l_v''|f\right)\\+(A^3-3AB^2)\mathrm{e}^{-B|l_i''-l_v'')|f}\sin\left(A|l_i''-l_v''|f\right)\\-(B^3-3A^2B)\mathrm{e}^{-B|l_i'-l_v''|f}\cos\left(A|l_i'-l_v''|f\right)\\-(A^3-3AB^2)\mathrm{e}^{-B|l_i'-l_v''|f}\sin\left(A|l_i'-l_v''|f\right)\\-(B^3-3A^2B)\mathrm{e}^{-B|l_i''-l_v'|f}\cos\left(A|l_i''-l_v'|f\right)\\-(A^3-3AB^2)\mathrm{e}^{-B|l_i''-l_v'|f}\sin\left(A|l_i''-l_v'|f\right)\end{bmatrix}$$

$$+\frac{1}{f^2(A^2+B^2)^2}\begin{bmatrix}(B^2-A^2)(l_v'-l_v)\mathrm{e}^{-B|l_i'-l_v'|f}\cos\left(A|l_i'-l_v'|f\right)\\-2AB(l_v'-l_v)\mathrm{e}^{-B|l_i'-l_v'|f}\sin\left(A|l_i'-l_v'|f\right)\\+(B^2-A^2)(l_v''-l_v)\mathrm{e}^{-B|l_i''-l_v''|f}\cos\left(A|l_i''-l_v''|f\right)\\-2AB(l_v''-l_v)\mathrm{e}^{-B|l_i''-l_v''|f}\sin\left(A|l_i''-l_v''|f\right)\\-(B^2-A^2)(l_v'-l_v)\mathrm{e}^{-B|l_i''-l_v'|f}\cos\left(A|l_i''-l_v'|f\right)\\+2AB(l_v'-l_v)\mathrm{e}^{-B|l_i''-l_v'|f}\sin\left(A|l_i''-l_v'|f\right)\\-(B^2-A^2)(l_v''-l_v)\mathrm{e}^{-B|l_i'-l_v''|f}\cos\left(A|l_i'-l_v''|f\right)\\+2AB(l_v''-l_v)\mathrm{e}^{-B|l_i'-l_v''|f}\sin(A|l_i'-l_v''|f)\end{bmatrix}$$

(A.1b)

$$\int_{l'_p}^{l''_p}\int_{l'_v}^{l''_v}(x_p-l_p)(x_v-l_v)\Psi(\xi_x,0,0)\mathrm{d}x_p\mathrm{d}x_v=\int_{l'_p}^{l''_p}\int_{l'_v}^{l''_v}(x_p-l_p)(x_v-l_v)\mathrm{e}^{-B\left|x_p-x_v\right|f}\cos\left(A(x_p-x_v)f\right)\mathrm{d}x_p\mathrm{d}x_v=$$

$$\frac{1}{f^4(A^2+B^2)^4}\begin{bmatrix}\left[(A^2-B^2)^2-4A^2B^2\right]\mathrm{e}^{-B\left|l'_p-l'_v\right|f}\cos\left(A\left|l'_p-l'_v\right|f\right)\\+\left[4AB(A^2-B^2)\right]\mathrm{e}^{-B\left|l'_p-l'_v\right|f}\sin\left(A\left|l'_p-l'_v\right|f\right)\\+\left[(A^2-B^2)^2-4A^2B^2\right]\mathrm{e}^{-B\left|l''_p-l''_v\right|f}\cos\left(A\left|l''_p-l''_v\right|f\right)\\+\left[4AB(A^2-B^2)\right]\mathrm{e}^{-B\left|l''_p-l''_v\right|f}\sin\left(A\left|l''_p-l''_v\right|f\right)\\-\left[(A^2-B^2)^2-4A^2B^2\right]\mathrm{e}^{-B\left|l''_p-l'_v\right|f}\cos\left(A\left|l''_p-l'_v\right|f\right)\\-\left[4AB(A^2-B^2)\right]\mathrm{e}^{-B\left|l''_p-l'_v\right|f}\sin\left(A\left|l''_p-l'_v\right|f\right)\\-\left[(A^2-B^2)^2-4A^2B^2\right]\mathrm{e}^{-B\left|l'_p-l''_v\right|f}\cos\left(A\left|l'_p-l''_v\right|f\right)\\-\left[4AB(A^2-B^2)\right]\mathrm{e}^{-B\left|l'_p-l''_v\right|f}\sin\left(A\left|l'_p-l''_v\right|f\right)\end{bmatrix}$$

$$+\frac{1}{f^3(A^2+B^2)^3}\begin{bmatrix}B(3A^2-B^2)(l_p+l_v-l'_p-l'_v)\mathrm{e}^{-B\left|l'_p-l'_v\right|f}\cos\left(A\left|l'_p-l'_v\right|f\right)\\+A(3B^2-A^2)(l_p+l_v-l'_p-l'_v)\mathrm{e}^{-B\left|l'_p-l'_v\right|f}\sin\left(A\left|l'_p-l'_v\right|f\right)\\+B(3A^2-B^2)(l_p+l_v-l''_p-l''_v)\mathrm{e}^{-B\left|l''_p-l''_v\right|f}\cos\left(A\left|l''_p-l''_v\right|f\right)\\+A(3B^2-A^2)(l_p+l_v-l''_p-l''_v)\mathrm{e}^{-B\left|l''_p-l''_v\right|f}\sin\left(A\left|l''_p-l''_v\right|f\right)\\-B(3A^2-B^2)(l_p+l_v-l''_p-l'_v)\mathrm{e}^{-B\left|l''_p-l'_v\right|f}\cos\left(A\left|l''_p-l'_v\right|f\right)\\-A(3B^2-A^2)(l_p+l_v-l''_p-l'_v)\mathrm{e}^{-B\left|l''_p-l'_v\right|f}\sin\left(A\left|l''_p-l'_v\right|f\right)\\-B(3A^2-B^2)(l_p+l_v-l'_p-l''_v)\mathrm{e}^{-B\left|l'_p-l''_v\right|f}\cos\left(A\left|l'_p-l''_v\right|f\right)\\-A(3B^2-A^2)(l_p+l_v-l'_p-l''_v)\mathrm{e}^{-B\left|l'_p-l''_v\right|f}\sin\left(A\left|l'_p-l''_v\right|f\right)\end{bmatrix}$$

$$+\frac{1}{f^2(A^2+B^2)^2}\times\begin{bmatrix}(B^2-A^2)(l_pl_v+l'_pl'_v-l'_pl_v-l_pl'_v)\mathrm{e}^{-B\left|l'_p-l'_v\right|f}\cos\left(A\left|l'_p-l'_v\right|f\right)\\-2AB(l_pl_v+l'_pl'_v-l'_pl_v-l_pl'_v)\mathrm{e}^{-B\left|l'_p-l'_v\right|f}\sin\left(A\left|l'_p-l'_v\right|f\right)\\+(B^2-A^2)(l_pl_v+l''_pl''_v-l''_pl_v-l_pl''_v)\mathrm{e}^{-B\left|l''_p-l''_v\right|f}\cos\left(A\left|l''_p-l''_v\right|f\right)\\-2AB(l_pl_v+l''_pl''_v-l''_pl_v-l_pl''_v)\mathrm{e}^{-B\left|l''_p-l''_v\right|f}\sin\left(A\left|l''_p-l''_v\right|f\right)\\-(B^2-A^2)(l_pl_v+l''_pl'_v-l''_pl_v-l_pl'_v)\mathrm{e}^{-B\left|l''_p-l'_v\right|f}\cos\left(A\left|l''_p-l'_v\right|f\right)\\+2AB(l_pl_v+l''_pl'_v-l''_pl_v-l_pl'_v)\mathrm{e}^{-B\left|l''_p-l'_v\right|f}\sin\left(A\left|l''_p-l'_v\right|f\right)\\-(B^2-A^2)(l_pl_v+l'_pl''_v-l'_pl_v-l_pl''_v)\mathrm{e}^{-B\left|l'_p-l''_v\right|f}\cos\left(A\left|l'_p-l''_v\right|f\right)\\+2AB(l_pl_v+l'_pl''_v-l'_pl_v-l_pl''_v)\mathrm{e}^{-B\left|l'_p-l''_v\right|f}\sin\left(A\left|l'_p-l''_v\right|f\right)\end{bmatrix} \tag{A.1c}$$

where $\xi_x=\left|x_i-x_u\right|$ (A.1d)

A.2. Integration of the lateral correlations in the y-direction

Substituting Eqs. (22b) and (22d) into Eqs. (21), (20) and (19) and then introducing the result into Eq. (17) and integrating over y to eliminate the space variable gives us expressions for the lateral correlations as follows:

$$\int_{d'_l}^{d''_l}\int_{d'_u}^{d''_u}\Psi(0,\xi_y,0)\mathrm{d}y_i\mathrm{d}y_u=\int_{d'_l}^{d''_l}\int_{d'_u}^{d''_u}\mathrm{e}^{\frac{-\alpha_y 2\pi\xi_y f}{U_c}}\mathrm{d}y_i dy_u$$

$$\int_{d'_l}^{d''_l}\int_{d'_u}^{d''_u}\mathrm{e}^{-C|y_i-y_u|f}\mathrm{d}y_i\mathrm{d}y_u=\frac{1}{C^2f^2}\left[\mathrm{e}^{-C|d'_i-d'_u|f}-\mathrm{e}^{-C|d''_i-d'_u|f}-\mathrm{e}^{-C|d'_i-d''_u|f}+\mathrm{e}^{-C|d''_i-d''_u|f}\right]$$

(A.2a)

$$\int_{d_i'}^{d_i''}\int_{d_k'}^{d_k''}(y_k-d_k)\Psi(0,\xi_y,0)\mathrm{d}y_i\mathrm{d}y_k=\int_{d_i'}^{d_i''}\int_{d_k'}^{d_k''}(y_k-d_k)\mathrm{e}^{-C|y_i-y_k|f}\mathrm{d}y_i\mathrm{d}y_k=$$

$$\frac{1}{C^3f^3}\left[\mathrm{e}^{-C|d_i'-d_k'|f}-\mathrm{e}^{-C|d_i''-d_k'|f}-\mathrm{e}^{-C|d_i'-d_k''|f}+\mathrm{e}^{-C|d_i''-d_k''|f}\right]+\frac{1}{C^2f^2}\times$$

$$\left[(d_k'-d_k)\mathrm{e}^{-C|d_i'-d_k'|f}-(d_k'-d_k)\mathrm{e}^{-C|d_i''-d_k'|f}-(d_k''-d_k)\mathrm{e}^{-C|d_i'-d_k''|f}+(d_k''-d_k)\mathrm{e}^{-C|d_i''-d_k''|f}\right]$$

(A.2b)

$$\int_{d_j'}^{d_j''}\int_{d_k'}^{d_k''}(y_j-d_j)(y_k-d_k)\Psi(0,\xi_y,0)\mathrm{d}y_j\mathrm{d}y_k=\int_{d_j'}^{d_j''}\int_{d_k'}^{d_k''}(y_j-d_j)(y_k-d_k)\mathrm{e}^{-C|y_j-y_k|f}\mathrm{d}y_j\mathrm{d}y_k=$$

$$\frac{1}{C^4f^4}\left[\mathrm{e}^{-C|d_j'-d_k'|f}-\mathrm{e}^{-C|d_j''-d_k'|f}-\mathrm{e}^{-C|d_j'-d_k''|f}+\mathrm{e}^{-C|d_j''-d_k''|f}\right]$$

$$+\frac{1}{C^3f^3}\begin{bmatrix}\mathrm{e}^{-C|d_j'-d_k'|f}(d_j'+d_k'-d_j-d_k)\\-\mathrm{e}^{-C|d_j''-d_k'|f}(d_j''+d_k'-d_j-d_k)\\-\mathrm{e}^{-C|d_j'-d_k''|f}(d_j'+d_k''-d_j-d_k)\\+\mathrm{e}^{-C|d_j''-d_k''|f}(d_j''+d_k''-d_j-d_k)\end{bmatrix}+\frac{1}{C^2f^2}\begin{bmatrix}\mathrm{e}^{-C|d_j'-d_k'|f}(d_j'd_k'-d_j'd_k-d_k'd_j+d_kd_j)\\-\mathrm{e}^{-C|d_j''-d_k'|f}(d_j''d_k'-d_j''d_k-d_k'd_j+d_kd_j)\\-\mathrm{e}^{-C|d_j'-d_k''|f}(d_j'd_k''-d_j'd_k-d_k''d_j+d_kd_j)\\+\mathrm{e}^{-C|d_j''-d_k''|f}(d_j''d_k''-d_j''d_k-d_k''d_j+d_kd_j)\end{bmatrix}$$

(A.2c)

where $\xi_y=|y_i-y_u|$ (A.2d)

Appendix B. Statements used in Eq. (26)

After introducing the expressions obtained from Sections *A.1* and *A.2* into Eq. (17) and integrating over frequency, Eq. (26) is obtained. Here Γ's are given as follows:

$$\Gamma_{iu} = \frac{K_2}{C^2(A^2+B^2)^2} \times$$

$$\left\{\begin{array}{l}
(B^2-A^2)\left[F_4^c(l_i',l_u',d_i',d_u')+F_4^c(l_i'',l_u'',d_i',d_u')-F_4^c(l_i',l_u'',d_i',d_u')-F_4^c(l_i'',l_u',d_i',d_u')\right] \\
-(2AB)\left[F_4^s(l_i',l_u',d_i',d_u')+F_4^s(l_i'',l_u'',d_i',d_u')-F_4^s(l_i',l_u'',d_i',d_u')-F_4^s(l_i'',l_u',d_i',d_u')\right] \\
+(B^2-A^2)\left[F_4^c(l_i',l_u',d_i'',d_u'')+F_4^c(l_i'',l_u'',d_i'',d_u'')-F_4^c(l_i',l_u'',d_i'',d_u'')-F_4^c(l_i'',l_u',d_i'',d_u'')\right] \\
-(2AB)\left[F_4^s(l_i',l_u',d_i'',d_u'')+F_4^s(l_i'',l_u'',d_i'',d_u'')-F_4^s(l_i',l_u'',d_i'',d_u'')-F_4^s(l_i'',l_u',d_i'',d_u'')\right] \\
-(B^2-A^2)\left[F_4^c(l_i',l_u',d_i'',d_u')+F_4^c(l_i'',l_u'',d_i'',d_u')-F_4^c(l_i',l_u'',d_i'',d_u')-F_4^c(l_i'',l_u',d_i'',d_u')\right] \\
+(2AB)\left[F_4^s(l_i',l_u',d_i'',d_u')+F_4^s(l_i'',l_u'',d_i'',d_u')-F_4^s(l_i',l_u'',d_i'',d_u')-F_4^s(l_i'',l_u',d_i'',d_u')\right] \\
-(B^2-A^2)\left[F_4^c(l_i',l_u',d_i',d_u'')+F_4^c(l_i'',l_u'',d_i',d_u'')-F_4^c(l_i',l_u'',d_i',d_u'')-F_4^c(l_i'',l_u',d_i',d_u'')\right] \\
+(2AB)\left[F_4^s(l_i',l_u',d_i',d_u'')+F_4^s(l_i'',l_u'',d_i',d_u'')-F_4^s(l_i',l_u'',d_i',d_u'')-F_4^s(l_i'',l_u',d_i',d_u'')\right]
\end{array}\right\},$$

(B.1)

$$\Gamma_{ik} = \frac{K_2}{C^3(A^2+B^2)^2} \times$$

$$\left\{ \begin{array}{l}
(B^2-A^2)\left[F_5^c(l_i',l_k',d_i',d_k') + F_5^c(l_i'',l_k'',d_i',d_k') - F_5^c(l_i',l_k'',d_i',d_k') - F_5^c(l_i'',l_k',d_i',d_k') \right] \\
-(2AB)\left[F_5^s(l_i',l_k',d_i',d_k') + F_5^s(l_i'',l_k'',d_i',d_k') - F_5^s(l_i',l_k'',d_i',d_k') - F_5^s(l_i'',l_k',d_i',d_k') \right] \\
+(B^2-A^2)\left[F_5^c(l_i',l_k',d_i'',d_k'') + F_5^c(l_i'',l_k'',d_i'',d_k'') - F_5^c(l_i',l_k'',d_i'',d_k'') - F_5^c(l_i'',l_k',d_i'',d_k'') \right] \\
-(2AB)\left[F_5^s(l_i',l_k',d_i'',d_k'') + F_5^s(l_i'',l_k'',d_i'',d_k'') - F_5^s(l_i',l_k'',d_i'',d_k'') - F_5^s(l_i'',l_k',d_i'',d_k'') \right] \\
-(B^2-A^2)\left[F_5^c(l_i',l_k',d_i'',d_k') + F_5^c(l_i'',l_k'',d_i'',d_k') - F_5^c(l_i',l_k'',d_i'',d_k') - F_5^c(l_i'',l_k',d_i'',d_k') \right] \\
+(2AB)\left[F_5^s(l_i',l_k',d_i'',d_k') + F_5^s(l_i'',l_k'',d_i'',d_k') - F_5^s(l_i',l_k'',d_i'',d_k') - F_5^s(l_i'',l_k',d_i'',d_k') \right] \\
-(B^2-A^2)\left[F_5^c(l_i',l_k',d_i',d_k'') + F_5^c(l_i'',l_k'',d_i',d_k'') - F_5^c(l_i',l_k'',d_i',d_k'') - F_5^c(l_i'',l_k',d_i',d_k'') \right] \\
+(2AB)\left[F_5^s(l_i',l_k',d_i',d_k'') + F_5^s(l_i'',l_k'',d_i',d_k'') - F_5^s(l_i',l_k'',d_i',d_k'') - F_5^s(l_i'',l_k',d_i',d_k'') \right]
\end{array} \right\}$$

$$+\frac{K_2}{C^2(A^2+B^2)^2}$$

$$\left\{ \begin{array}{l}
(B^2-A^2)(d_k'-d_k)\left[F_4^c(l_i',l_k',d_i',d_k') + F_4^c(l_i'',l_k'',d_i',d_k') - F_4^c(l_i',l_k'',d_i',d_k') - F_4^c(l_i'',l_k',d_i',d_k') \right] \\
-(2AB)(d_k'-d_k)\ \left[F_4^s(l_i',l_k',d_i',d_k') + F_4^s(l_i'',l_k'',d_i',d_k') - F_4^s(l_i',l_k'',d_i',d_k') - F_4^s(l_i'',l_k',d_i',d_k') \right] \\
+(B^2-A^2)(d_k''-d_k)\left[F_4^c(l_i',l_k',d_i'',d_k'') + F_4^c(l_i'',l_k'',d_i'',d_k'') - F_4^c(l_i',l_k'',d_i'',d_k'') - F_4^c(l_i'',l_k',d_i'',d_k'') \right] \\
-(2AB)(d_k''-d_k)\ \left[F_4^s(l_i',l_k',d_i'',d_k'') + F_4^s(l_i'',l_k'',d_i'',d_k'') - F_4^s(l_i',l_k'',d_i'',d_k'') - F_4^s(l_i'',l_k',d_i'',d_k'') \right] \\
-(B^2-A^2)(d_k'-d_k)\left[F_4^c(l_i',l_k',d_i'',d_k') + F_4^c(l_i'',l_k'',d_i'',d_k') - F_4^c(l_i',l_k'',d_i'',d_k') - F_4^c(l_i'',l_k',d_i'',d_k') \right] \\
+(2AB)(d_k'-d_k)\left[F_4^s(l_i',l_k',d_i'',d_k') + F_4^s(l_i'',l_k'',d_i'',d_k') - F_4^s(l_i',l_k'',d_i'',d_k') - F_4^s(l_i'',l_k',d_i'',d_k') \right] \\
-(B^2-A^2)(d_k''-d_k)\left[F_4^c(l_i',l_k',d_i',d_k'') + F_4^c(l_i'',l_k'',d_i',d_k'') - F_4^c(l_i',l_k'',d_i',d_k'') - F_4^c(l_i'',l_k',d_i',d_k'') \right] \\
+(2AB)(d_k''-d_k)\left[F_4^s(l_i',l_k',d_i',d_k'') + F_4^s(l_i'',l_k'',d_i',d_k'') - F_4^s(l_i',l_k'',d_i',d_k'') - F_4^s(l_i'',l_k',d_i',d_k'') \right]
\end{array} \right\}$$

(B.2)

$$\Gamma_{iv} = \frac{K_2}{C^2(A^2+B^2)^3}\left\{\begin{array}{l}(B^3-3A^2B)\times\\ \left[F_5^c(l_i',l_v',d_i',d_v')+F_5^c(l_i'',l_v'',d_i',d_v')-F_5^c(l_i',l_v'',d_i',d_v')-F_5^c(l_i'',l_v',d_i',d_v')\right]\\ +(A^3-3AB^2)\times\\ \left[F_5^s(l_i',l_v',d_i',d_v')+F_5^s(l_i'',l_v'',d_i',d_v')-F_5^s(l_i',l_v'',d_i',d_v')-F_5^s(l_i'',l_v',d_i',d_v')\right]\end{array}\right\}$$

$$+\frac{K_2}{C^2(A^2+B^2)^2}\left\{\begin{array}{l}(B^2-A^2)(l_v''-l_v)\times\\ \left[F_4^c(l_i'',l_v'',d_i',d_v')-F_4^c(l_i',l_v'',d_i',d_v')\right]\\ +(B^2-A^2)(l_v'-l_v)\times\\ \left[F_4^c(l_i',l_v',d_i',d_v')-F_4^c(l_i'',l_v',d_i',d_v')\right]\\ -2AB(l_v''-l_v)\left[F_4^s(l_i'',l_v'',d_i',d_v')-F_4^s(l_i',l_v'',d_i',d_v')\right]\\ -2AB(l_v'-l_v)\left[F_4^s(l_i',l_v',d_i',d_v')-F_4^s(l_i'',l_v',d_i',d_v')\right]\end{array}\right\}$$

$$+\frac{K_2}{C^2(A^2+B^2)^3}\left\{\begin{array}{l}(B^3-3A^2B)\times\\ \left[F_5^c(l_i',l_v',d_i'',d_v'')+F_5^c(l_i'',l_v'',d_i'',d_v'')-F_5^c(l_i',l_v'',d_i'',d_v'')-F_5^c(l_i'',l_v',d_i'',d_v'')\right]\\ +(A^3-3AB^2)\times\\ \left[F_5^s(l_i',l_v',d_i'',d_v'')+F_5^s(l_i'',l_v'',d_i'',d_v'')-F_5^s(l_i',l_v'',d_i'',d_v'')-F_5^s(l_i'',l_v',d_i'',d_v'')\right]\end{array}\right\}$$

$$+\frac{K_2}{C^2(A^2+B^2)^2}\left\{\begin{array}{l}(B^2-A^2)(l_v''-l_v)\left[F_4^c(l_i'',l_v'',d_i'',d_v'')-F_4^c(l_i',l_v'',d_i'',d_v'')\right]\\ +(B^2-A^2)(l_v'-l_v)\left[F_4^c(l_i',l_v',d_i'',d_v'')-F_4^c(l_i'',l_v',d_i'',d_v'')\right]\\ -2AB(l_v''-l_v)\left[F_4^s(l_i'',l_v'',d_i'',d_v'')-F_4^s(l_i',l_v'',d_i'',d_v'')\right]\\ -2AB(l_v'-l_v)\left[F_4^s(l_i',l_v',d_i'',d_v'')-F_4^s(l_i'',l_v',d_i'',d_v'')\right]\end{array}\right\}$$

$$+\frac{K_2}{C^2(A^2+B^2)^3}\left\{\begin{array}{l}-(B^3-3A^2B)\times\\ \left[F_5^c(l_i',l_v',d_i',d_v'')+F_5^c(l_i'',l_v'',d_i',d_v'')-F_5^c(l_i',l_v'',d_i',d_v'')-F_5^c(l_i'',l_v',d_i',d_v'')\right]\\ -(A^3-3AB^2)\times\\ \left[F_5^s(l_i',l_v',d_i',d_v'')+F_5^s(l_i'',l_v'',d_i',d_v'')-F_5^s(l_i',l_v'',d_i',d_v'')-F_5^s(l_i'',l_v',d_i',d_v'')\right]\end{array}\right\}$$

$$+\frac{K_2}{C^2(A^2+B^2)^2}\left\{\begin{array}{l}-(B^2-A^2)(l_v''-l_v)\left[F_4^c(l_i'',l_v'',d_i',d_v'')-F_4^c(l_i',l_v'',d_i',d_v'')\right]\\ -(B^2-A^2)(l_v'-l_v)\left[F_4^c(l_i',l_v',d_i',d_v'')-F_4^c(l_i'',l_v',d_i',d_v'')\right]\\ +2AB(l_v''-l_v)\left[F_4^s(l_i'',l_v'',d_i',d_v'')-F_4^s(l_i',l_v'',d_i',d_v'')\right]\\ +2AB(l_v'-l_v)\left[F_4^s(l_i',l_v',d_i',d_v'')-F_4^s(l_i'',l_v',d_i',d_v'')\right]\end{array}\right\}$$

$$+\frac{K_2}{C^2(A^2+B^2)^3}\left\{\begin{array}{l}-(B^3-3A^2B)\times\\ \left[F_5^c(l_i',l_v',d_i'',d_v')+F_5^c(l_i'',l_v'',d_i'',d_v')-F_5^c(l_i',l_v'',d_i'',d_v')-F_5^c(l_i'',l_v',d_i'',d_v')\right]\\ -(A^3-3AB^2)\times\\ \left[F_5^s(l_i',l_v',d_i'',d_v')+F_5^s(l_i'',l_v'',d_i'',d_v')-F_5^s(l_i',l_v'',d_i'',d_v')-F_5^s(l_i'',l_v',d_i'',d_v')\right]\end{array}\right\}$$

$$+\frac{K_2}{C^2(A^2+B^2)^2}\left\{\begin{array}{l}-(B^2-A^2)(l_v''-l_v)\left[F_4^c(l_i'',l_v'',d_i'',d_v')-F_4^c(l_i',l_v'',d_i'',d_v')\right]\\-(B^2-A^2)(l_v'-l_v)\left[F_4^c(l_i',l_v',d_i'',d_v')-F_4^c(l_i'',l_v',d_i'',d_v')\right]\\+2AB(l_v''-l_v)\left[F_4^s(l_i'',l_v'',d_i'',d_v')-F_4^s(l_i',l_v'',d_i'',d_v')\right]\\+2AB(l_v'-l_v)\left[F_4^s(l_i',l_v',d_i'',d_v')-F_4^s(l_i'',l_v',d_i'',d_v')\right]\end{array}\right\} \quad \text{(B.3)}$$

$$\Gamma_{jk} = \frac{K_2}{C^4(A^2+B^2)^2} \times$$

$$\begin{Bmatrix}
(B^2-A^2)\left[F_6^c(l'_j,l'_k,d'_j,d'_k)+F_6^c(l''_j,l''_k,d'_j,d'_k)-F_6^c(l'_j,l''_k,d'_j,d'_k)-F_6^c(l''_j,l'_k,d'_j,d'_k)\right] \\
-2AB\left[F_6^s(l'_j,l'_k,d'_j,d'_k)+F_6^s(l''_j,l''_k,d'_j,d'_k)-F_6^s(l'_j,l''_k,d'_j,d'_k)-F_6^s(l''_j,l'_k,d'_j,d'_k)\right] \\
+(B^2-A^2)\left[F_6^c(l'_j,l'_k,d''_j,d''_k)+F_6^c(l''_j,l''_k,d''_j,d''_k)-F_6^c(l'_j,l''_k,d''_j,d''_k)-F_6^c(l''_j,l'_k,d''_j,d''_k)\right] \\
-2AB\left[F_6^s(l'_j,l'_k,d''_j,d''_k)+F_6^s(l''_j,l''_k,d''_j,d''_k)-F_6^s(l'_j,l''_k,d''_j,d''_k)-F_6^s(l''_j,l'_k,d''_j,d''_k)\right] \\
-(B^2-A^2)\left[F_6^c(l'_j,l'_k,d''_j,d'_k)+F_6^c(l''_j,l''_k,d''_j,d'_k)-F_6^c(l'_j,l''_k,d''_j,d'_k)-F_6^c(l''_j,l'_k,d''_j,d'_k)\right] \\
+2AB\left[F_6^s(l'_j,l'_k,d''_j,d'_k)+F_6^s(l''_j,l''_k,d''_j,d'_k)-F_6^s(l'_j,l''_k,d''_j,d'_k)-F_6^s(l''_j,l'_k,d''_j,d'_k)\right] \\
-(B^2-A^2)\left[F_6^c(l'_j,l'_k,d'_j,d''_k)+F_6^c(l''_j,l''_k,d'_j,d''_k)-F_6^c(l'_j,l''_k,d'_j,d''_k)-F_6^c(l''_j,l'_k,d'_j,d''_k)\right] \\
+2AB\left[F_6^s(l'_j,l'_k,d'_j,d''_k)+F_6^s(l''_j,l''_k,d'_j,d''_k)-F_6^s(l'_j,l''_k,d'_j,d''_k)-F_6^s(l''_j,l'_k,d'_j,d''_k)\right]
\end{Bmatrix}$$

$$+\frac{K_2}{C^3(A^2+B^2)^2}$$

$$\begin{Bmatrix}
(B^2-A^2)(d'_j+d'_k-d_j-d_k)\left[F_5^c(l'_j,l'_k,d'_j,d'_k)+F_5^c(l''_j,l''_k,d'_j,d'_k)-F_5^c(l'_j,l''_k,d'_j,d'_k)-F_5^c(l''_j,l'_k,d'_j,d'_k)\right] \\
-2AB(d'_j+d'_k-d_j-d_k)\left[F_5^s(l'_j,l'_k,d'_j,d'_k)+F_5^s(l''_j,l''_k,d'_j,d'_k)-F_5^s(l'_j,l''_k,d'_j,d'_k)-F_5^s(l''_j,l'_k,d'_j,d'_k)\right] \\
+(B^2-A^2)(d''_j+d''_k-d_j-d_k)\left[F_5^c(l'_j,l'_k,d''_j,d''_k)+F_5^c(l''_j,l''_k,d''_j,d''_k)-F_5^c(l'_j,l''_k,d''_j,d''_k)-F_5^c(l''_j,l'_k,d''_j,d''_k)\right] \\
-2AB(d''_j+d''_k-d_j-d_k)\left[F_5^s(l'_j,l'_k,d''_j,d''_k)+F_5^s(l''_j,l''_k,d''_j,d''_k)-F_5^s(l'_j,l''_k,d''_j,d''_k)-F_5^s(l''_j,l'_k,d''_j,d''_k)\right] \\
-(B^2-A^2)(d''_j+d'_k-d_j-d_k)\left[F_5^c(l'_j,l'_k,d''_j,d'_k)+F_5^c(l''_j,l''_k,d''_j,d'_k)-F_5^c(l'_j,l''_k,d''_j,d'_k)-F_5^c(l''_j,l'_k,d''_j,d'_k)\right] \\
+2AB(d''_j+d'_k-d_j-d_k)\left[F_5^s(l'_j,l'_k,d''_j,d'_k)+F_5^s(l''_j,l''_k,d''_j,d'_k)-F_5^s(l'_j,l''_k,d''_j,d'_k)-F_5^s(l''_j,l'_k,d''_j,d'_k)\right] \\
-(B^2-A^2)(d'_j+d''_k-d_j-d_k)\left[F_5^c(l'_j,l'_k,d'_j,d''_k)+F_5^c(l''_j,l''_k,d'_j,d''_k)-F_5^c(l'_j,l''_k,d'_j,d''_k)-F_5^c(l''_j,l'_k,d'_j,d''_k)\right] \\
+2AB(d'_j+d''_k-d_j-d_k)\left[F_5^s(l'_j,l'_k,d'_j,d''_k)+F_5^s(l''_j,l''_k,d'_j,d''_k)-F_5^s(l'_j,l''_k,d'_j,d''_k)-F_5^s(l''_j,l'_k,d'_j,d''_k)\right]
\end{Bmatrix}$$

$$+\frac{K_2}{C^2(A^2+B^2)^2}$$

$$\begin{Bmatrix}
(B^2-A^2)(d'_jd'_k-d'_jd_k-d'_kd_j+d_jd_k)\left[F_4^c(l'_j,l'_k,d'_j,d'_k)+F_4^c(l''_j,l''_k,d'_j,d'_k)-F_4^c(l'_j,l''_k,d'_j,d'_k)-F_4^c(l''_j,l'_k,d'_j,d'_k)\right] \\
-2AB(d'_jd'_k-d'_jd_k-d'_kd_j+d_jd_k)\left[F_4^s(l'_j,l'_k,d'_j,d'_k)+F_4^s(l''_j,l''_k,d'_j,d'_k)-F_4^s(l'_j,l''_k,d'_j,d'_k)-F_4^s(l''_j,l'_k,d'_j,d'_k)\right] \\
+(B^2-A^2)(d''_jd''_k-d''_jd_k-d''_kd_j+d_jd_k)\left[F_4^c(l'_j,l'_k,d''_j,d''_k)+F_4^c(l''_j,l''_k,d''_j,d''_k)-F_4^c(l'_j,l''_k,d''_j,d''_k)-F_4^c(l''_j,l'_k,d''_j,d''_k)\right] \\
-2AB(d''_jd''_k-d''_jd_k-d''_kd_j+d_jd_k)\left[F_4^s(l'_j,l'_k,d''_j,d''_k)+F_4^s(l''_j,l''_k,d''_j,d''_k)-F_4^s(l'_j,l''_k,d''_j,d''_k)-F_4^s(l''_j,l'_k,d''_j,d''_k)\right] \\
-(B^2-A^2)(d''_jd'_k-d''_jd_k-d'_kd_j+d_jd_k)\left[F_4^c(l'_j,l'_k,d''_j,d'_k)+F_4^c(l''_j,l''_k,d''_j,d'_k)-F_4^c(l'_j,l''_k,d''_j,d'_k)-F_4^c(l''_j,l'_k,d''_j,d'_k)\right] \\
+2AB(d''_jd'_k-d''_jd_k-d'_kd_j+d_jd_k)\left[F_4^s(l'_j,l'_k,d''_j,d'_k)+F_4^s(l''_j,l''_k,d''_j,d'_k)-F_4^s(l'_j,l''_k,d''_j,d'_k)-F_4^s(l''_j,l'_k,d''_j,d'_k)\right] \\
-(B^2-A^2)(d'_jd''_k-d'_jd_k-d''_kd_j+d_jd_k)\left[F_4^c(l'_j,l'_k,d'_j,d''_k)+F_4^c(l''_j,l''_k,d'_j,d''_k)-F_4^c(l'_j,l''_k,d'_j,d''_k)-F_4^c(l''_j,l'_k,d'_j,d''_k)\right] \\
+2AB(d'_jd''_k-d'_jd_k-d''_kd_j+d_jd_k)\left[F_4^s(l'_j,l'_k,d'_j,d''_k)+F_4^s(l''_j,l''_k,d'_j,d''_k)-F_4^s(l'_j,l''_k,d'_j,d''_k)-F_4^s(l''_j,l'_k,d'_j,d''_k)\right]
\end{Bmatrix}$$

(B.4)

$$\Gamma_{pk}=\frac{K_2}{C^3(A^2+B^2)^3}\times$$

$$\left\{\begin{array}{l}
(B^3-3A^2B)\left[F_6^c(l'_p,l'_k,d'_p,d'_k)+F_6^c(l''_p,l''_k,d'_p,d'_k)-F_6^c(l'_p,l''_k,d'_p,d'_k)-F_6^c(l''_p,l'_k,d'_p,d'_k)\right]\\
+(A^3-3AB^2)\left[F_6^s(l'_p,l'_k,d'_p,d'_k)+F_6^s(l''_p,l''_k,d'_p,d'_k)-F_6^s(l'_p,l''_k,d'_p,d'_k)-F_6^s(l''_p,l'_k,d'_p,d'_k)\right]\\
+(B^3-3A^2B)\left[F_6^c(l'_p,l'_k,d''_p,d''_k)+F_6^c(l''_p,l''_k,d''_p,d''_k)-F_6^c(l'_p,l''_k,d''_p,d''_k)-F_6^c(l''_p,l'_k,d''_p,d''_k)\right]\\
+(A^3-3AB^2)\left[F_6^s(l'_p,l'_k,d''_p,d''_k)+F_6^s(l''_p,l''_k,d''_p,d''_k)-F_6^s(l'_p,l''_k,d''_p,d''_k)-F_6^s(l''_p,l'_k,d''_p,d''_k)\right]\\
-(B^3-3A^2B)\left[F_6^c(l'_p,l'_k,d''_p,d'_k)+F_6^c(l''_p,l''_k,d''_p,d'_k)-F_6^c(l'_p,l''_k,d''_p,d'_k)-F_6^c(l''_p,l'_k,d''_p,d'_k)\right]\\
-(A^3-3AB^2)\left[F_6^s(l'_p,l'_k,d''_p,d'_k)+F_6^s(l''_p,l''_k,d''_p,d'_k)-F_6^s(l'_p,l''_k,d''_p,d'_k)-F_6^s(l''_p,l'_k,d''_p,d'_k)\right]\\
-(B^3-3A^2B)\left[F_6^c(l'_p,l'_k,d'_p,d''_k)+F_6^c(l''_p,l''_k,d'_p,d''_k)-F_6^c(l'_p,l''_k,d'_p,d''_k)-F_6^c(l''_p,l'_k,d'_p,d''_k)\right]\\
-(A^3-3AB^2)\left[F_6^s(l'_p,l'_k,d'_p,d''_k)+F_6^s(l''_p,l''_k,d'_p,d''_k)-F_6^s(l'_p,l''_k,d'_p,d''_k)-F_6^s(l''_p,l'_k,d'_p,d''_k)\right]
\end{array}\right\}$$

$$+\frac{K_2(d'_k-d_k)}{C^2(A^2+B^2)^3}\times$$

$$\left\{\begin{array}{l}
(B^3-3A^2B)\left[F_5^c(l'_p,l'_k,d'_p,d'_k)+F_5^c(l''_p,l''_k,d'_p,d'_k)-F_5^c(l'_p,l''_k,d'_p,d'_k)-F_5^c(l''_p,l'_k,d'_p,d'_k)\right]\\
+(A^3-3AB^2)\left[F_5^s(l'_p,l'_k,d'_p,d'_k)+F_5^s(l''_p,l''_k,d'_p,d'_k)-F_5^s(l'_p,l''_k,d'_p,d'_k)-F_5^s(l''_p,l'_k,d'_p,d'_k)\right]
\end{array}\right\}$$

$$+\frac{K_2(d''_k-d_k)}{C^2(A^2+B^2)^3}\times$$

$$\left\{\begin{array}{l}
(B^3-3A^2B)\left[F_5^c(l'_p,l'_k,d''_p,d''_k)+F_5^c(l''_p,l''_k,d''_p,d''_k)-F_5^c(l'_p,l''_k,d''_p,d''_k)-F_5^c(l''_p,l'_k,d''_p,d''_k)\right]\\
+(A^3-3AB^2)\left[F_5^s(l'_p,l'_k,d''_p,d''_k)+F_5^s(l''_p,l''_k,d''_p,d''_k)-F_5^s(l'_p,l''_k,d''_p,d''_k)-F_5^s(l''_p,l'_k,d''_p,d''_k)\right]
\end{array}\right\}$$

$$-\frac{K_2(d'_k-d_k)}{C^2(A^2+B^2)^3}\times$$

$$\left\{\begin{array}{l}
(B^3-3A^2B)\left[F_5^c(l'_p,l'_k,d''_p,d'_k)+F_5^c(l''_p,l''_k,d''_p,d'_k)-F_5^c(l'_p,l''_k,d''_p,d'_k)-F_5^c(l''_p,l'_k,d''_p,d'_k)\right]\\
+(A^3-3AB^2)\left[F_5^s(l'_p,l'_k,d''_p,d'_k)+F_5^s(l''_p,l''_k,d''_p,d'_k)-F_5^s(l'_p,l''_k,d''_p,d'_k)-F_5^s(l''_p,l'_k,d''_p,d'_k)\right]
\end{array}\right\}$$

$$-\frac{K_2(d''_k-d_k)}{C^2(A^2+B^2)^3}\times$$

$$\left\{\begin{array}{l}
(B^3-3A^2B)\left[F_5^c(l'_p,l'_k,d'_p,d''_k)+F_5^c(l''_p,l''_k,d'_p,d''_k)-F_5^c(l'_p,l''_k,d'_p,d''_k)-F_5^c(l''_p,l'_k,d'_p,d''_k)\right]\\
+(A^3-3AB^2)\left[F_5^s(l'_p,l'_k,d'_p,d''_k)+F_5^s(l''_p,l''_k,d'_p,d''_k)-F_5^s(l'_p,l''_k,d'_p,d''_k)-F_5^s(l''_p,l'_k,d'_p,d''_k)\right]
\end{array}\right\}$$

$$+\frac{K_2}{C^3(A^2+B^2)^2}\left\{\begin{array}{l}
(B^2-A^2)(l'_p-l_p)\left[F_5^c(l'_p,l'_k,d'_p,d'_k)-F_5^c(l'_p,l''_k,d'_p,d'_k)\right]\\
+(B^2-A^2)(l''_p-l_p)\left[F_5^c(l''_p,l''_k,d'_p,d'_k)-F_5^c(l''_p,l'_k,d'_p,d'_k)\right]\\
-2AB(l'_p-l_p)\left[F_5^s(l'_p,l'_k,d'_p,d'_k)-F_5^s(l'_p,l''_k,d'_p,d'_k)\right]\\
-2AB(l''_p-l_p)\left[F_5^s(l''_p,l''_k,d'_p,d'_k)-F_5^s(l''_p,l'_k,d'_p,d'_k)\right]
\end{array}\right\}$$

$$+\frac{K_2}{C^3(A^2+B^2)^2}\left\{\begin{array}{l}(B^2-A^2)(l'_p-l_p)\left[F_5^c(l'_p,l'_k,d''_p,d''_k)-F_5^c(l'_p,l''_k,d''_p,d''_k)\right]\\+(B^2-A^2)(l''_p-l_p)\left[F_5^c(l''_p,l''_k,d''_p,d''_k)-F_5^c(l''_p,l'_k,d''_p,d''_k)\right]\\-2AB(l'_p-l_p)\left[F_5^s(l'_p,l'_k,d''_p,d''_k)-F_5^s(l'_p,l''_k,d''_p,d''_k)\right]\\-2AB(l''_p-l_p)\left[F_5^s(l''_p,l''_k,d''_p,d''_k)-F_5^s(l''_p,l'_k,d''_p,d''_k)\right]\end{array}\right\}$$

$$-\frac{K_2}{C^3(A^2+B^2)^2}\left\{\begin{array}{l}(B^2-A^2)(l'_p-l_p)\left[F_5^c(l'_p,l'_k,d''_p,d'_k)-F_5^c(l'_p,l''_k,d''_p,d'_k)\right]\\+(B^2-A^2)(l''_p-l_p)\left[F_5^c(l''_p,l''_k,d''_p,d'_k)-F_5^c(l''_p,l'_k,d''_p,d'_k)\right]\\-2AB(l'_p-l_p)\left[F_5^s(l'_p,l'_k,d''_p,d'_k)-F_5^s(l'_p,l''_k,d''_p,d'_k)\right]\\-2AB(l''_p-l_p)\left[F_5^s(l''_p,l''_k,d''_p,d'_k)-F_5^s(l''_p,l'_k,d''_p,d'_k)\right]\end{array}\right\}$$

$$-\frac{K_2}{C^3(A^2+B^2)^2}\left\{\begin{array}{l}(B^2-A^2)(l'_p-l_p)\left[F_5^c(l'_p,l'_k,d'_p,d''_k)-F_5^c(l'_p,l''_k,d'_p,d''_k)\right]\\+(B^2-A^2)(l''_p-l_p)\left[F_5^c(l''_p,l''_k,d'_p,d''_k)-F_5^c(l''_p,l'_k,d'_p,d''_k)\right]\\-2AB(l'_p-l_p)\left[F_5^s(l'_p,l'_k,d'_p,d''_k)-F_5^s(l'_p,l''_k,d'_p,d''_k)\right]\\-2AB(l''_p-l_p)\left[F_5^s(l''_p,l''_k,d'_p,d''_k)-F_5^s(l''_p,l'_k,d'_p,d''_k)\right]\end{array}\right\}$$

$$+\frac{K_2(d'_k-d_k)}{C^2(A^2+B^2)^2}\left\{\begin{array}{l}(B^2-A^2)(l'_p-l_p)\left[F_4^c(l'_p,l'_k,d'_p,d'_k)-F_4^c(l'_p,l''_k,d'_p,d'_k)\right]\\+(B^2-A^2)(l''_p-l_p)\left[F_4^c(l''_p,l''_k,d'_p,d'_k)-F_4^c(l''_p,l'_k,d'_p,d'_k)\right]\\-2AB(l'_p-l_p)\left[F_4^s(l'_p,l'_k,d'_p,d'_k)-F_4^s(l'_p,l''_k,d'_p,d'_k)\right]\\-2AB(l''_p-l_p)\left[F_4^s(l''_p,l''_k,d'_p,d'_k)-F_4^s(l''_p,l'_k,d'_p,d'_k)\right]\end{array}\right\}$$

$$+\frac{K_2(d''_k-d_k)}{C^2(A^2+B^2)^2}\left\{\begin{array}{l}(B^2-A^2)(l'_p-l_p)\left[F_4^c(l'_p,l'_k,d''_p,d''_k)-F_4^c(l'_p,l''_k,d''_p,d''_k)\right]\\+(B^2-A^2)(l''_p-l_p)\left[F_4^c(l''_p,l''_k,d''_p,d''_k)-F_4^c(l''_p,l'_k,d''_p,d''_k)\right]\\-2AB(l'_p-l_p)\left[F_4^s(l'_p,l'_k,d''_p,d''_k)-F_4^s(l'_p,l''_k,d''_p,d''_k)\right]\\-2AB(l''_p-l_p)\left[F_4^s(l''_p,l''_k,d''_p,d''_k)-F_4^s(l''_p,l'_k,d''_p,d''_k)\right]\end{array}\right\}$$

$$-\frac{K_2(d'_k-d_k)}{C^2(A^2+B^2)^2}\left\{\begin{array}{l}(B^2-A^2)(l'_p-l_p)\left[F_4^c(l'_p,l'_k,d''_p,d'_k)-F_4^c(l'_p,l''_k,d''_p,d'_k)\right]\\+(B^2-A^2)(l''_p-l_p)\left[F_4^c(l''_p,l''_k,d''_p,d'_k)-F_4^c(l''_p,l'_k,d''_p,d'_k)\right]\\-2AB(l'_p-l_p)\left[F_4^s(l'_p,l'_k,d''_p,d'_k)-F_4^s(l'_p,l''_k,d''_p,d'_k)\right]\\-2AB(l''_p-l_p)\left[F_4^s(l''_p,l''_k,d''_p,d'_k)-F_4^s(l''_p,l'_k,d''_p,d'_k)\right]\end{array}\right\}$$

$$-\frac{K_2(d_k''-d_k)}{C^2(A^2+B^2)^2}\left\{\begin{array}{l}(B^2-A^2)(l_p'-l_p)\left[F_4^c(l_p',l_k',d_p',d_k'')-F_4^c(l_p',l_k'',d_p',d_k'')\right]\\+(B^2-A^2)(l_p''-l_p)\left[F_4^c(l_p'',l_k'',d_p',d_k'')-F_4^c(l_p'',l_k',d_p',d_k'')\right]\\-2AB(l_p'-l_p)\left[F_4^s(l_p',l_k',d_p',d_k'')-F_4^s(l_p',l_k'',d_p',d_k'')\right]\\-2AB(l_p''-l_p)\left[F_4^s(l_p'',l_k'',d_p',d_k'')-F_4^s(l_p'',l_k',d_p',d_k'')\right]\end{array}\right\} \tag{B.5}$$

$$
\begin{aligned}
\Gamma_{pv} = {} & \frac{K_2}{C^2(A^2+B^2)^4}\times \\
& \left\{ \begin{array}{l}
\left[(A^2-B^2)^2-4A^2B^2\right]\left[F_6^c(l'_p,l'_v,d'_p,d'_v)+F_6^c(l''_p,l''_v,d'_p,d'_v)-F_6^c(l'_p,l''_v,d'_p,d'_v)-F_6^c(l''_p,l'_v,d'_p,d'_v)\right] \\
+\left[4AB(A^2-B^2)\right]\left[F_6^s(l'_p,l'_v,d'_p,d'_v)+F_6^s(l''_p,l''_v,d'_p,d'_v)-F_6^s(l'_p,l''_v,d'_p,d'_v)-F_6^s(l''_p,l'_v,d'_p,d'_v)\right] \\
+\left[(A^2-B^2)^2-4A^2B^2\right]\left[F_6^c(l'_p,l'_v,d''_p,d''_v)+F_6^c(l''_p,l''_v,d''_p,d''_v)-F_6^c(l'_p,l''_v,d''_p,d''_v)-F_6^c(l''_p,l'_v,d''_p,d''_v)\right] \\
+\left[4AB(A^2-B^2)\right]\left[F_6^s(l'_p,l'_v,d''_p,d''_v)+F_6^s(l''_p,l''_v,d''_p,d''_v)-F_6^s(l'_p,l''_v,d''_p,d''_v)-F_6^s(l''_p,l'_v,d''_p,d''_v)\right] \\
-\left[(A^2-B^2)^2-4A^2B^2\right]\left[F_6^c(l'_p,l'_v,d''_p,d'_v)+F_6^c(l''_p,l''_v,d''_p,d'_v)-F_6^c(l'_p,l''_v,d''_p,d'_v)-F_6^c(l''_p,l'_v,d''_p,d'_v)\right] \\
-\left[4AB(A^2-B^2)\right]\left[F_6^s(l'_p,l'_v,d''_p,d'_v)+F_6^s(l''_p,l''_v,d''_p,d'_v)-F_6^s(l'_p,l''_v,d''_p,d'_v)-F_6^s(l''_p,l'_v,d''_p,d'_v)\right] \\
-\left[(A^2-B^2)^2-4A^2B^2\right]\left[F_6^c(l'_p,l'_v,d'_p,d''_v)+F_6^c(l''_p,l''_v,d'_p,d''_v)-F_6^c(l'_p,l''_v,d'_p,d''_v)-F_6^c(l''_p,l'_v,d'_p,d''_v)\right] \\
-\left[4AB(A^2-B^2)\right]\left[F_6^c(l'_p,l'_v,d'_p,d''_v)+F_6^c(l''_p,l''_v,d'_p,d''_v)-F_6^c(l'_p,l''_v,d'_p,d''_v)-F_6^c(l''_p,l'_v,d'_p,d''_v)\right]
\end{array} \right\} \\
& +\frac{K_2}{C^2(A^2+B^2)^3}\times \\
& \left\{ \begin{array}{l}
B(3A^2-B^2)(l_p+l_v-l'_p-l'_v)\left[F_5^c(l'_p,l'_v,d'_p,d'_v)+F_5^c(l'_p,l'_v,d''_p,d''_v)-F_5^c(l'_p,l'_v,d'_p,d''_v)-F_5^c(l'_p,l'_v,d''_p,d'_v)\right] \\
+A(3B^2-A^2)(l_p+l_v-l'_p-l'_v)\left[F_5^s(l'_p,l'_v,d'_p,d'_v)+F_5^s(l'_p,l'_v,d''_p,d''_v)-F_5^s(l'_p,l'_v,d'_p,d''_v)-F_5^s(l'_p,l'_v,d''_p,d'_v)\right] \\
+B(3A^2-B^2)(l_p+l_v-l''_p-l''_v)\left[F_5^c(l''_p,l''_v,d'_p,d'_v)+F_5^c(l''_p,l''_v,d''_p,d''_v)-F_5^c(l''_p,l''_v,d'_p,d''_v)-F_5^c(l''_p,l''_v,d''_p,d'_v)\right] \\
+A(3B^2-A^2)(l_p+l_v-l''_p-l''_v)\left[F_5^s(l''_p,l''_v,d'_p,d'_v)+F_5^s(l''_p,l''_v,d''_p,d''_v)-F_5^s(l''_p,l''_v,d'_p,d''_v)-F_5^s(l''_p,l''_v,d''_p,d'_v)\right] \\
-B(3A^2-B^2)(l_p+l_v-l''_p-l'_v)\left[F_5^c(l''_p,l'_v,d'_p,d'_v)+F_5^c(l''_p,l'_v,d''_p,d''_v)-F_5^c(l''_p,l'_v,d'_p,d''_v)-F_5^c(l''_p,l'_v,d''_p,d'_v)\right] \\
-A(3B^2-A^2)(l_p+l_v-l''_p-l'_v)\left[F_5^s(l''_p,l'_v,d'_p,d'_v)+F_5^s(l''_p,l'_v,d''_p,d''_v)-F_5^s(l''_p,l'_v,d'_p,d''_v)-F_5^s(l''_p,l'_v,d''_p,d'_v)\right] \\
-B(3A^2-B^2)(l_p+l_v-l'_p-l''_v)\left[F_5^c(l'_p,l''_v,d'_p,d'_v)+F_5^c(l'_p,l''_v,d''_p,d''_v)-F_5^c(l'_p,l''_v,d'_p,d''_v)-F_5^c(l'_p,l''_v,d''_p,d'_v)\right] \\
-A(3B^2-A^2)(l_p+l_v-l'_p-l''_v)\left[F_5^s(l'_p,l''_v,d'_p,d'_v)+F_5^s(l'_p,l''_v,d''_p,d''_v)-F_5^s(l'_p,l''_v,d'_p,d''_v)-F_5^s(l'_p,l''_v,d''_p,d'_v)\right]
\end{array} \right\} \\
& +\frac{K_2}{C^2(A^2+B^2)^2}\times \\
& \left\{ \begin{array}{l}
(B^2-A^2)(l_pl_v+l'_pl'_v-l'_pl_v-l_pl'_v)\left[F_4^c(l'_p,l'_v,d'_p,d'_v)+F_4^c(l'_p,l'_v,d''_p,d''_v)-F_4^c(l'_p,l'_v,d'_p,d''_v)-F_4^c(l'_p,l'_v,d''_p,d'_v)\right] \\
-2AB(l_pl_v+l'_pl'_v-l'_pl_v-l_pl'_v)\left[F_4^s(l'_p,l'_v,d'_p,d'_v)+F_4^s(l'_p,l'_v,d''_p,d''_v)-F_4^s(l'_p,l'_v,d'_p,d''_v)-F_4^s(l'_p,l'_v,d''_p,d'_v)\right] \\
+(B^2-A^2)(l_pl_v+l''_pl''_v-l''_pl_v-l_pl''_v)\left[F_4^c(l''_p,l''_v,d'_p,d'_v)+F_4^c(l''_p,l''_v,d''_p,d''_v)-F_4^c(l''_p,l''_v,d'_p,d''_v)-F_4^c(l''_p,l''_v,d''_p,d'_v)\right] \\
-2AB(l_pl_v+l''_pl''_v-l''_pl_v-l_pl''_v)\left[F_4^s(l''_p,l''_v,d'_p,d'_v)+F_4^s(l''_p,l''_v,d''_p,d''_v)-F_4^s(l''_p,l''_v,d'_p,d''_v)-F_4^s(l''_p,l''_v,d''_p,d'_v)\right] \\
-(B^2-A^2)(l_pl_v+l''_pl'_v-l''_pl_v-l_pl'_v)\left[F_4^c(l''_p,l'_v,d'_p,d'_v)+F_4^c(l''_p,l'_v,d''_p,d''_v)-F_4^c(l''_p,l'_v,d'_p,d''_v)-F_4^c(l''_p,l'_v,d''_p,d'_v)\right] \\
+2AB(l_pl_v+l''_pl'_v-l''_pl_v-l_pl'_v)\left[F_4^s(l''_p,l'_v,d'_p,d'_v)+F_4^s(l''_p,l'_v,d''_p,d''_v)-F_4^s(l''_p,l'_v,d'_p,d''_v)-F_4^s(l''_p,l'_v,d''_p,d'_v)\right] \\
-(B^2-A^2)(l_pl_v+l'_pl''_v-l'_pl_v-l_pl''_v)\left[F_4^c(l'_p,l''_v,d'_p,d'_v)+F_4^c(l'_p,l''_v,d''_p,d''_v)-F_4^c(l'_p,l''_v,d'_p,d''_v)-F_4^c(l'_p,l''_v,d''_p,d'_v)\right] \\
+2AB(l_pl_v+l'_pl''_v-l'_pl_v-l_pl''_v)\left[F_4^s(l'_p,l''_v,d'_p,d'_v)+F_4^s(l'_p,l''_v,d''_p,d''_v)-F_4^s(l'_p,l''_v,d'_p,d''_v)-F_4^s(l'_p,l''_v,d''_p,d'_v)\right]
\end{array} \right\}
\end{aligned}
\tag{B.6}
$$

Appendix C. Functions used in Appendix B

$$F_4^c(l_i',l_u',d_i',d_u') = \int_0^\infty \frac{\mathrm{e}^{-\left[K_1+C\left|d_i'-d_u'\right|+B\left|l_i'-l_u'\right|\right]f}\cos(A\left|l_i'-l_u'\right|f)}{f^4\left[\dfrac{f^4}{f_r^4}+(\dfrac{4{\zeta_r}^2-2}{f_r^2})f^2+1\right]}\mathrm{d}f$$

$$= \frac{\pi}{8f_r^3}\left(5\mathrm{e}^{-\gamma_1}\sin\gamma_2 - 5\mathrm{e}^{-\gamma_3}\sin\gamma_4 + \frac{1}{\zeta_r}\left(\mathrm{e}^{-\gamma_1}\cos\gamma_2 + \mathrm{e}^{-\gamma_3}\cos\gamma_4\right)\right),$$

(C.1)

$$F_4^S(l_i',l_u',d_i',d_u') = \int_0^\infty \frac{\mathrm{e}^{-\left[K_1+C\left|d_i'-d_u'\right|+B\left|l_i'-l_u'\right|\right]f}\sin(A\left|l_i'-l_u'\right|f)}{f^4\left[\dfrac{f^4}{f_r^4}+(\dfrac{4{\zeta_r}^2-2}{f_r^2})f^2+1\right]}\mathrm{d}f$$

$$= \frac{\pi}{8f_r^3}\left(-5\mathrm{e}^{-\gamma_1}\cos\gamma_2 + 5\mathrm{e}^{-\gamma_3}\cos\gamma_4 + \frac{1}{\zeta_r}\left(\mathrm{e}^{-\gamma_1}\sin\gamma_2 + \mathrm{e}^{-\gamma_3}\sin\gamma_4\right)\right),$$

(C.2)

$$F_5^c(l_i',l_v',d_i',d_v') = \int_0^\infty \frac{\mathrm{e}^{-\left[K_1+C\left|d_i'-d_v'\right|+B\left|l_i'-l_v'\right|\right]f}\cos(A\left|l_i'-l_v'\right|f)}{f^5\left[\dfrac{f^4}{f_r^4}+(\dfrac{4{\zeta_r}^2-2}{f_r^2})f^2+1\right]}\mathrm{d}f$$

$$= \frac{\pi}{8f_r^4}\left(6\mathrm{e}^{-\gamma_1}\sin\gamma_2 - 6\mathrm{e}^{-\gamma_3}\sin\gamma_4 + \frac{1}{\zeta_r}\left(\mathrm{e}^{-\gamma_1}\cos\gamma_2 + \mathrm{e}^{-\gamma_3}\cos\gamma_4\right)\right)$$

(C.3)

$$F_5^s(l_i',l_v',d_i',d_v') = \int_0^\infty \frac{e^{-\left[K_1+C\left|d_i'-d_v'\right|+B\left|l_i'-l_v'\right|\right]f}\sin(A\left|l_i'-l_v'\right|f)}{f^5\left[\frac{f^4}{f_r^4}+(\frac{4{\zeta_r}^2-2}{f_r^2})f^2+1\right]}df$$

$$= \frac{\pi}{8f_r^4}\left(-6e^{-\gamma_1}\cos\gamma_2 + 6e^{-\gamma_3}\cos\gamma_4 + \frac{1}{\zeta_r}\left(e^{-\gamma_1}\sin\gamma_2 + e^{-\gamma_3}\sin\gamma_4\right)\right) \tag{C.4}$$

$$F_6^c(l_p',l_k',d_p',d_k') = \int_0^\infty \frac{e^{-\left[K_1+C\left|d_p'-d_k'\right|+B\left|l_p'-l_k'\right|\right]f}\cos(A\left|l_p'-l_k'\right|f)}{f^6\left[\frac{f^4}{f_r^4}+(\frac{4{\zeta_r}^2-2}{f_r^2})f^2+1\right]}df$$

$$= \frac{\pi}{8f_r^5}\left(7e^{-\gamma_1}\sin\gamma_2 - 7e^{-\gamma_3}\sin\gamma_4 + \frac{1}{\zeta_r}\left(e^{-\gamma_1}\cos\gamma_2 + e^{-\gamma_3}\cos\gamma_4\right)\right) \tag{C.5}$$

$$F_6^s(l_p',l_k',d_p',d_k') = \int_0^\infty \frac{e^{-\left[K_1+C\left|d_p'-d_k'\right|+B\left|l_p'-l_k'\right|\right]f}\sin(A\left|l_p'-l_k'\right|f)}{f^6\left[\frac{f^4}{f_r^4}+(\frac{4{\zeta_r}^2-2}{f_r^2})f^2+1\right]}df$$

$$= \frac{\pi}{8f_r^5}\left(-7e^{-\gamma_1}\cos\gamma_2 + 7e^{-\gamma_3}\cos\gamma_4 + \frac{1}{\zeta_r}\left(e^{-\gamma_1}\sin\gamma_2 + e^{-\gamma_3}\sin\gamma_4\right)\right) \tag{C.6}$$

and

$$\gamma_1(l_i',l_u',d_i',d_u') = \left[K_1 + C\left|d_i'-d_u'\right| + (A\zeta_r + B)\left|l_i'-l_u'\right|\right]f_r, \tag{C.7}$$

$$\gamma_2(l_i',l_u',d_i',d_u') = \left[-K_1\zeta_r - C\zeta_r\left|d_i'-d_u'\right| + (A - B\zeta_r)\left|l_i'-l_u'\right|\right]f_r, \tag{C.8}$$

$$\gamma_3(l_i',l_u',d_i',d_u') = \left[K_1 + C\left|d_i'-d_u'\right| - (A\zeta_r - B)\left|l_i'-l_u'\right|\right]f_r, \tag{C.9}$$

$$\gamma_4(l_i', l_u', d_i', d_u') = \left[K_1\zeta_r + C\zeta_r \left| d_i' - d_u' \right| + (A + B\zeta_r) \left| l_i' - l_u' \right| \right] f_r , \quad \text{(C.10)}$$

where the constants are given as follows:

$$A = \frac{2\pi}{U_c},\ B = \frac{\alpha_x 2\pi}{U_c},\ C = \frac{\alpha_y 2\pi}{U_c},$$

$$K_1 = \frac{k_1 \delta^*}{U_\infty},\ K_2 = k_2 \rho_f^2 \delta^* U_\infty^3,$$

where f is the forced frequency in Hz, f_r is the rth natural frequency in Hz, ζ_r is the rth damping ratio, l_i' and l_i'' are the limits of the area surrounding the node i in the x-direction, d_i' and d_i'' are the limits of the area surrounding the node i in the y-direction, U_c is the convection velocity, U_∞ is the free stream velocity, ρ_f is the density of the fluid, δ^* is the boundary layer displacement thickness, k_1=0.25, k_2=2×10^{-6}, α_x = 0.116 and α_y = 0.7.

References

[1] G.M. Corcos, Resolution of pressure in turbulence, *Journal of the Acoustical Society of America* 35 (2) (1963) 192-199.

[2] G.M. Corcos, The resolution of turbulent pressures at the wall of a boundary layer, *Journal of Sound and Vibration* 6 (1) (1967) 59-70.

[3] L. Maestrello, Design criterion of panel structure excited by turbulent boundary layer, *Journal of Aircraft* 5 (4) (1968) 321-328.

[4] T.M. Farabee, M.J. Casarella, Spectral features of wall pressure fluctuations beneath turbulent boundary layers, *Physics of Fluids* 3 (1991) 2410-2420.

[5] H.P. Bakewell, G.F. Carey, J.J. Libuka, H.H. Schloemer, W.A. Von Winkle, Wall pressure correlations in turbulent pipe flow, Report No. 559, U. S. Navy Underwater Sound Laboratory, 1962.

[6] G.M. Corcos, Structure of turbulent pressure field in boundary-layer flows, *Journal of Fluid Mechanics* 18 (3) (1964) 353-378.

[7] W.W. Willmarth, C.E. Wooldridge, Measurements of fluctuating pressure at wall beneath thick turbulent boundary layer, *Journal of Fluid Mechanics* 14 (2) (1962) 187-210.

[8] M.K. Bull, Wall-pressure fluctuations associated with subsonic turbulent boundary layer flow, *Journal of Fluid Mechanics* 28 (4) (1967) 719-764.

[9] W.K. Blake, *Mechanics of Flow-Induced Sound and Vibration, Vol. II: Complex Flow-Structure Interaction*, Academic Press, London, 1986.

[10] M.G. Cottis, J.G. Jasonides, The response of a finite thin cylindrical shell to random pressure fields, *Proceeding of the Second International Conference on Acoustical fatigue in Aerospace structures*, Dayton, Ohio, USA, April 29-May 1, 1964, pp. 185-212.

[11] M.G. Cottis, On the dynamic response of an orthotropic finite cylindrical shell to an arbitrary pressure field, *Journal of Sound and Vibration* 7 (1) (1968) 31-38.

[12] J.M. Clinch, Prediction and measurement of the vibrations induced in thin-walled pipes by the passage of internal turbulent water flow, *Journal of Sound and Vibration* 12 (1970) 429-451.

[13] A.A. Lakis, M.P. Païdoussis, Prediction of the response of a cylindrical shell to arbitrary or boundary-layer-induced random pressure fields, *Journal of Sound and Vibration* 25 (1) (1972) 1-27.

[14] L.R. Curling, M.P. Païdoussis, Analyses for random flow-induced vibration of cylindrical structures subjected to turbulent axial flow, *Journal of Sound and Vibration* 264 (4) (2003) 795-833.

[15] F. Birgersson, N.S. Ferguson, S. Finnveden, Application of the spectral finite element method to turbulent boundary layer induced vibration of plates, *Journal of Sound and Vibration* 259 (4) (2003) 873-891.

[16] S. Finnveden, F. Birgersson, U. Ross, T. Kremer, A model of wall pressure correlation for prediction of turbulence-induced vibration, *Journal of Fluids and Structures* 20 (8) (2005) 1127-1143.

[17] D. Mazzoni, An efficient approximation for the vibro-acoustic response of a turbulent boundary layer excited panel, *Journal of Sound and Vibration* 264 (4) (2003) 951-971.

[18] P. Vitiello, S. De Rosa, F. Franco, Convected field analysis of flat panels response to turbulent boundary layer induced excitation, *Aerospace Science and Technology* 12 (1) (2008) 91-104.

[19] S. De Rosa, F. Franco, Exact and numerical responses of a plate under a turbulent boundary layer excitation, *Journal of Fluids and Structures* 24 (2) (2008) 212-230.

[20] S.A. Hambric, Y.F. Hwang, W.K. Bonness, Vibrations of plates with clamped and free edges excited by low-speed turbulent boundary layer flow, *Journal of Fluids and Structures* 19 (1) (2004) 93-110.

[21] A.A. Lakis, M.P. Païdoussis, Free vibration of cylindrical shells partially filled with liquid, *Journal of Sound and Vibration* 19 (1) (1971) 1-15.

[22] A.A. Lakis, M.P. Païdoussis, Dynamic analysis of axially non-uniform thin cylindrical shells, *Journal of Mechanical Engineering Science* 14 (1) (1972) 49-71.

[23] Y. Kerboua, A.A. Lakis, M. Thomas, L. Marcouiller, Hybrid method for vibration analysis of rectangular plates, *Nuclear Engineering and Design* 237 (8) (2007) 791-801.

[24] Y. Kerboua, A.A. Lakis, M. Thomas, L. Marcouiller, Vibration analysis of rectangular plates coupled with fluid, *Applied Mathematical Modelling* 32 (12) (2008) 2570-2586.

[25] M. Esmailzadeh, A.A. Lakis, M. Thomas, L. Marcouiller, Three-dimensional modeling of curved structures containing and/or submerged in fluid, *Finite Elements in Analysis and Design* 44 (6-7) (2008) 334-345.

[26] F.M. White, A unified theory of turbulent wall pressure fluctuations, Report No. 629, USN Underwater Sound Laboratory, 1964.

[27] H.P. Bakewell, Turbulent wall-pressure fluctuations on a body of revolution, *Journal of the Acoustical Society of America* 43 (6) (1968) 1358-1363.

[28] J.M. Clinch, Study of vibrations induced in thin-walled pipes under varying flow conditions, NASA-CR-86659, IIT Research Institute, Fluid Dynamics Section, 1967.

[29] W.W. Willmarth, C.E. Wooldridge, Measurements of correlation between fluctuating velocities and fluctuating wall pressure in thick turbulent boundary layer, Report No. 456, North Atlantic Treaty Organization, Paris, 1963.

[30] H.P. Bakewell, Narrow-band investigations of the longitudinal space-time correlation function in turbulent airflow, *Journal of the Acoustical Society of America* 36 (1) (1964) 146-148.

[31] W.W. Willmarth, C.S. Young, Wall pressure fluctuations beneath turbulent boundary layers on a flat plate and a cylinder, *Journal of Fluid Mechanics* 41 (1) (1970) 47-80.

[32] J.M. Clinch, Measurements of wall pressure field at surface of smooth-walled pipe containing turbulent water flow, *Journal of Sound and Vibration* 9 (3) (1969) 398-419.

[33] M.K. Au-Yang, *Flow-Induced Vibration of Power and Process Plant Components*, ASME Press, New York, 2001.

[34] H. Schlichting, *Boundary-Layer Theory*, McGraw-Hill, New York, 1979.

[35] M.R. Haddara, S. Cao, A study of the dynamic response of submerged rectangular flat plates, *Marine Structures* 9 (10) (1996) 913-933.

L'École Polytechnique se spécialise dans la formation d'ingénieurs et la recherche en ingénierie depuis 1873

École Polytechnique de Montréal

École affiliée à l'Université de Montréal

Campus de l'Université de Montréal
C.P. 6079, succ. Centre-ville
Montréal (Québec)
Canada H3C 3A7

www.polymtl.ca

ÉCOLE
POLYTECHNIQUE
MONTRÉAL